Total RNA extraction and real-time PCR

Total RNA was isolated from the cell/gel mixture with Isogen following the supplier's protocol. Complementary DNA (cDNA) was synthesized from 1 μg of total RNA with the Superscript II reverse transcriptase kit (Invitrogen, Carlsbad, CA). For real-time PCR, the ABI Prism Sequence Detection System 7000 was used. Aliquots of first-strand cDNA (1 μg) were amplified with the QuantiTect SYBER Green PCR Kit (Qiagen, Osaka, Japan) under the following conditions: initial denaturation for 10 min at 94°C followed by 40 cycles consisting of 15 s at 94°C and 1 min at 60°C. Data analysis consisted of fold induction; the expression ratio was calculated from the differences in threshold cycles at which an increase in reporter fluorescence above a baseline signal could first be detected among three samples and was averaged for duplicate experiments. The sequence of primers we used in real-time PCR to detect Col1A1, Col2A1, β1 integrin, N-cadherin, and GAPDH were as follows:

Col1A1 F:5′-CTCCTCGCTTTCCTTCCTCT-3′, R:5′-GTGCTAAAGGTGCCAATGG T-3′; Col2A1 F:5′-GAGTCAAGGGTGATCGTGGT-3′, R: 5′-CACCTTGGTCTCCA GAAGGA-3′[22]; β1integrin F: 5′-AGTTGCAGTTTGTGGATCACTGAT-3′, R: 5′-AAA GTGAAACCCGGCATCTG-3′[23]; N-cadherin; F: 5′-GTGCCATTAGCCAAG GGATTCAGC-3′, R: 5′–GCGTTCCTGTTCCACTCATAGGAGG-3′[24]; GAPDH F: 5′-GAAGGT GAAGGTCGGAGTCA-3′, R: 5′-GAAGATGGTGATGGGATTTC-3′. GAPDH was used as the housekeeping gene.

Biochemical measurement of glycosaminoglycan and collagen types I and II

We evaluated the glycosaminoglycan (GAG) content using the Alcian blue-binding assay (Wieslab AB, Lund, Sweden), according to the supplier's protocol. After digestion in 0.3% collagenase for 1 h at 37°C, cell debris and insoluble material were removed by centrifugation at 6000*g* for 30 min. GAG in the supernatant was precipitated with Alcian blue solution, and the sediments after centrifugation at 6000*g* for 15 min were dissolved again in 4*M* GuHCl-33% propanol solution. The spectrophotometric absorbance of the mixture was measured at a wavelength of 600 nm.

The collagen proteins of the cell/gel construct were solubilized and quantified in ELISA according to the protocol of human Type I, II Collagen Detection Kit (Chondrex, Redmound, WA). The cell/gel construct was dissolved in 10 mg/mL pepsin/0.05*M* acetic acid at 4°C for 48 h and then in 1 mg/mL pancreatic elastase/1×TSB at 4°C overnight. In the mixture, the collagen proteins were captured by polyclonal anti-human type I or type II collagen antibodies and detected by biotinylated counterparts and streptavidin peroxidase. OPD and H_2O_2 were added to the mixture and the spectrophotometric absorbance of the mixture was measured at a wavelength of 490 nm.

Histology

The cell/gel constructs were fixed with 4% paraformaldehyde in 0.1*M* phosphate buffer (pH 7.4) for 2 h in 4°C and immersed in 10% sucrose in phosphate-buffered saline (PBS), 20% sucrose in PBS, and a 2:1 mixture of 20% sucrose in PBS and OCT compound in succession with rapid freezing with liquid nitrogen in preparation for cryosection. For the alginate, 0.1*M* cacodylate buffer containing 102 m*M* $CaCl_2$ was used instead of phosphate buffer or PBS. The specimens were cryosectioned at a thickness of 10 μm and were stained with toluidine blue-O.

Young's modulus of each hydrogel

Five hundred microliter of each hydrogel at 0.5% weight was prepared in three wells of a 24-well plate, and was incubated in 0.5 mL of DMEM/F-12 for 24 h in 37°C. After removal of medium, Young's modulus of each hydrogel was measured with a Venustron tactile sensor (Axiom, Fukushima, Japan). Under computer control, the motor-driven sensor unit automatically presses down on the surface of materials and provides an indentation force and a decrease in the resonant frequency. The resonant frequency of the sensor was set to 50 Hz, while the maximum depth of indentation was 1 mm. Young's modulus can be calculated by the indentation force and the decrease of the resonant frequency, based on the principles reported by Aoyagi and Yoshida.[25] The software Venus 42 provided by the manufacturer was used for calculation. Young's modulus was measured 9 times in three wells for each hydrogel.

RESULTS

Chondrocyte proliferation

At first, we examined the effects of atelopeptide collagen, alginate, and PuraMatrix™ on chondrocyte proliferation. Human auricular chondrocytes of Passage 2 were encapsulated in the three kinds of hydrogel materials and cultured for 2 weeks. The chondrocytes in atelopeptide collagen proliferated at ~10-fold with 10% FBS, although no proliferation was seen without FBS. The cells rather decreased in number with or without FBS, in alginate or PuraMatrix™ (Fig. 1).

Gene expression of chondrocytes in each hydrogel

Next, we observed the effects of those hydrogel materials on the gene expression of chondrocytes when the dedifferentiated chondrocytes (Passage 4) were embedded in the hydrogel at a high cell density of 10^7 cells/mL. At 1 week after incubation, the expression of Col1A1 in all of hydrogel materials ranged between half and 2-fold of that in high density culture without any hydrogel (gel(−)), when they were incu-

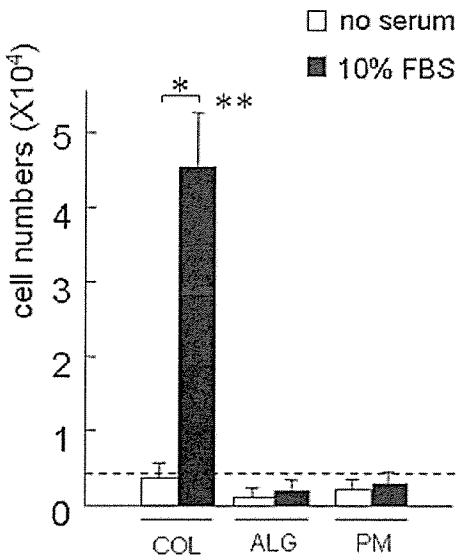

Figure 1. Effects of atelopeptide collagen, alginate, or PuraMatrix™ hydrogel on chondrocyte proliferation. In the atelopepide collagen (COL), chondrocytes of Passage 2 effectively increased in numbers not without (blank bar), but with (filled) FBS. The cell numbers in alginate (ALG) or PuraMatrix™ (PM) rather decreased either with or without FBS. The broken line indicates the number of chondrocytes at the start of incubation. All values are presented as mean plus standard deviation. Statistics were assessed using the Student t test (*: $p < 0.05$ with *vs.* without FBS; **: $p < 0.05$ when compared with alginate and PuraMatrix™).

bated in medium without any factors (control). Because of the induction of redifferentiation by a medium containing insulin and BMP-2, the Col1A1 expression in all hydrogels decreased, when compared with that in the control medium.

The expression of Col2A1 was more than 100 times larger than that of gel(−), when the cells were embedded in every kind of hydrogel material, even in the control medium. With the redifferentiation medium, those in all hydrogel exhibited over a 10^5 fold increase, when compared with that of gel(−). Among the three kinds of materials, the expression of both Col1A1 and Col2A1 in PuraMatrix™ tended to be high in the control medium, but response to the redifferentiation medium was rather low in Col2A1 expression (Fig. 2).

To examine the molecular effects of the hydrogel on chondrocytes, we measured the gene expression of β1 integrin and N-cadherin, which play major roles in cell–matrix interactions and cell-to-cell contacts, respectively, in chondrocytes.[20,21] At 1 week, β1 integrin was abundantly expressed in gel(−). Within all kinds of hydrogel materials, the β1 integrin expression was upregulated in the redifferentiation medium when compared with that in the control. β1 integrin of the atelopeptide collagen constructs showed the highest expression among three materials, not only in the redifferentiation media, but also in the control, suggesting abundant extracellular signaling through chondrocyte/collagen interaction. The enhancement of β1 integrin expression in both control and redifferentiation media seemed lower within PuraMatrix™ than within atelopeptide collagen, although PuraMatrix™ abundantly contains the RAD motif, which is regarded as the analog of RGD, the major integrin ligand in collagen.[16] Alginate did not enhance β1 in-

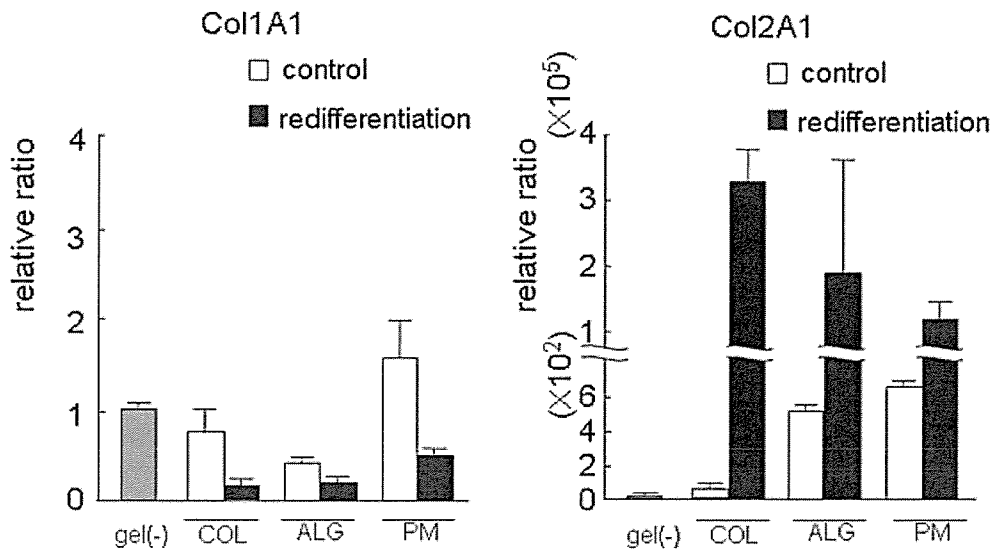

Figure 2. Gene expression of collagen types I and II in chondrocytes within each hydrogel. Within all hydrogel materials, the expression of Col2A1 was promoted in the redifferentiation medium (filled bar), when compared with the control (blank bar), although that of Col1A1 expression was decreased. The expression in the high-cell density culture without any hydrogel (gel(−)) was standardized to 1 (grey bar). All values are presented as mean plus standard deviation. COL, ateloeptide collagen; ALG, alginate; PM, PuraMatrix™.

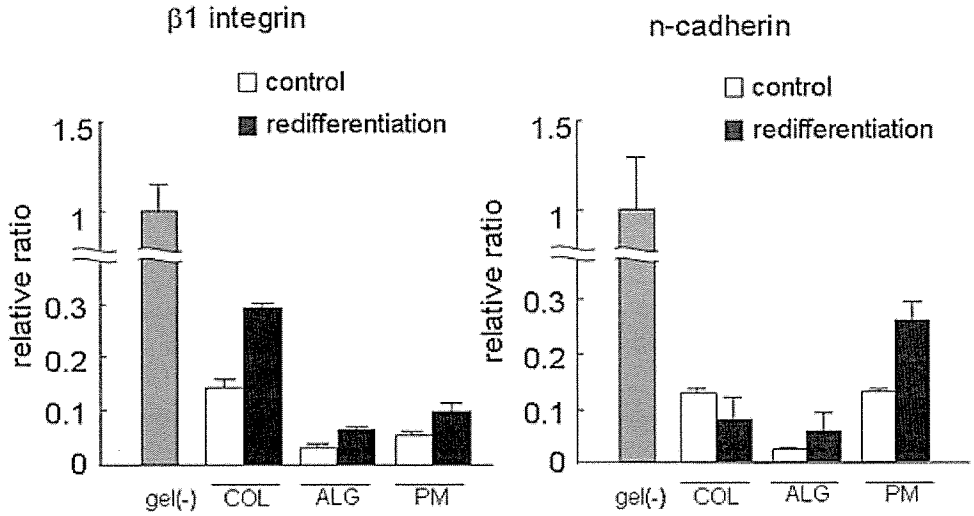

Figure 3. Gene expression of β1 integrin and N-cadherin in chondrocytes within each hydrogel. The atelopeptide collagen showed high expression of β1 integrin, not only in the redifferentiation media (filled bar), but also in the control (blank bar), although the alginate did not promote β1 integrin expression. The expression of N-cadherin was also inhibited within the alginate in both the control and redifferentiation media. The expression of high-cell density culture without any hydrogel (gel(−)) was standardized to 1 (grey bar). All values are presented as mean plus standard deviation. COL, ateloeptide collagen; ALG, alginate; PM, PuraMatrix™.

tegrin expression, perhaps due to the lack of cell–matrix interactions (Fig. 3, left).

Although the expression of N-cadherin was enhanced in the gel(−), its expression decreased in all hydrogel materials. Particularly, the upregulation of N-cadherin expression was inhibited within alginate in both control and redifferentiation media, suggesting that alginate can maintain isolation of each chondrocyte. In the atelopeptide collagen, although both control and redifferentiation media promoted N-cadherin expression when compared with that in alginate, it was downregulated according to the induction of redifferentiation. Contrarily, the chondrocytes in PuraMatrix™ rather increased the expression of N-cadherin, when the redifferentiation was induced (Fig. 3, right).

Matrix synthesis of chondrocytes in each hydrogel

At 3 weeks after the incubation of chondrocytes at a high density (10^7/mL), gel(−) accumulated collagen type I, although it was diminished in encapsulation with each hydrogel. Moreover, the protein content of collagen type I was decreased in the atelopeptide collagen and in PuraMatrix™ with the redifferentiation media, when compared with that in the control. The content of collagen type II or GAG in gel(−) and each hydrogel was hardly detectable in the control medium, but the redifferentiation medium significantly gained amounts of GAG and collagen type II, in all hydrogels. The accumulation of collagen type II was remarkable in the redifferentiation medium within the atelopeptide collagen hydrogel, while the GAG content was abundantly determined in alginate. Also in PuraMatrix™, the effects of the redifferentiation medium were noted on the synthesis of collagen type II and GAG, although the amount of both matrices was less than that in atelopeptide collagen or alginate (Fig. 4).

The constructs of chondrocytes with encapsulation in atelopeptide collagen, alginate, and PuraMatrix™ were examined histologically. All the constructs were metachromatically stained with toluidine blue, when they were cultured in the redifferentiation media. However, the findings for PuraMatrix™ showed a sparse and loose appearance in the middle area of the constructs, even in the redifferentiation medium, suggesting that the ability to support cells and newly-synthesized matrices in PuraMatrix™ was weak (Fig. 5). The aggregation of high-cell density culture without any hydrogel (gel(−)) was too small in size and too fragile to be prepared for histological examination.

Mechanical properties

While the hydrogel of atelopeptide collagen or alginate was firm, the PuraMatrix™ gel seemed rather soft when the hydrogel was probed by the tip of a microspatula. To examine mechanical properties of each hydrogel quantitatively, we measured Young's modulus by a Venustron tactile sensor. Each hydrogel reached maximal elasticity within 24 h of incubation in the culture media. Young's modulus of atelopeptide collagen was the highest (65.5 ± 4.1 kPa), following

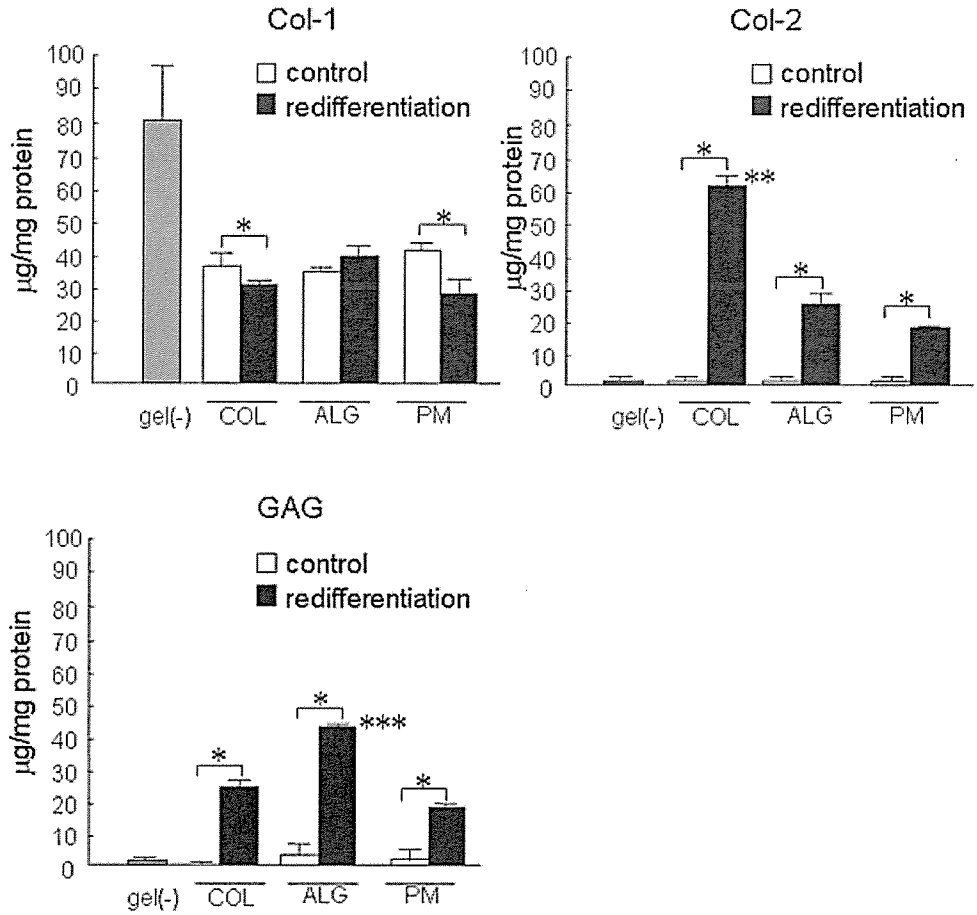

Figure 4. Matrix synthesis of chondrocytes in each hydrogel. Amounts of collagen type II and GAG were increased in the redifferentiation medium (filled bar), when compared with the control (blank bar), within all materials. The amount of collagen type I was decreased in the atelopeptide collagen (COL) and the alginate (ALG) hydrogel. All values are presented as mean plus standard deviation. Statistics were assessed using the Student t test (*: $p < 0.01$ control *vs.* redifferentiation; **: $p < 0.01$ when compared with alginate and PuraMatrix™ (PM); ***: $p < 0.01$ when compared with collagen and PuraMatrix™). Gray bar: high-cell density culture without any hydrogel (gel(−)).

those of alginate (36.3 ± 5.4 kPa) and PuraMatrix™ (16.7 ± 1.0 kPa) (Fig. 6).

DISCUSSION AND CONCLUSIONS

Chondrocytes in native cartilage are surrounded by an abundant extracellular matrix in all directions and are isolated into their own lacunae. This implies that chondrocytes are constantly exposed to cell–matrix interactions, and in contrast, that they are separated from each other to lose cell-to-cell contacts under physiological conditions. Cell–matrix interaction is essential for chondrocyte proliferation, differentiation, or survival.[26] Integrins are a major class of cell adhesion molecules and are expressed in chondrocytes. They consist of α/β heterodimers that associate with intracellular proteins on ligand binding.[27] Chondrocytes dominantly contain α1β1, α3β1, α5β1, α10β1, αvβ3, and αvβ5 integrins.[28] Integrins recognize the peptide motif "RGD" commonly contained in several extracellular matrix proteins such as fibronectin, collagen, and vitronectin. After engagement with the extracellular matrix components, integrin receives signal via multiple downstream effectors, including integrin-linked kinase (ILK), and exerts various functions. Mice with a chondrocyte-specific disruption of the gene encoding ILK by Cre-LoxP system developed chondrodysplasia, caused by impaired chondrocyte proliferation.[29,30]

The atelopeptides of type I collagen are a fiber protein made from a collagen, which is solubilized by protease.[31] The atelopeptide collagen seems to possess the ligands for integrins, RGD. In the present study, chondrocytes embedded in the atelopeptide collagen hydrogel proliferated rapidly with FBS and produced abundant collagen type II and GAG. This may suggest that the support or stimulation of cell growth and matrix synthesis is related to cell–matrix interaction through RGD-integrin signaling. On the other hand,

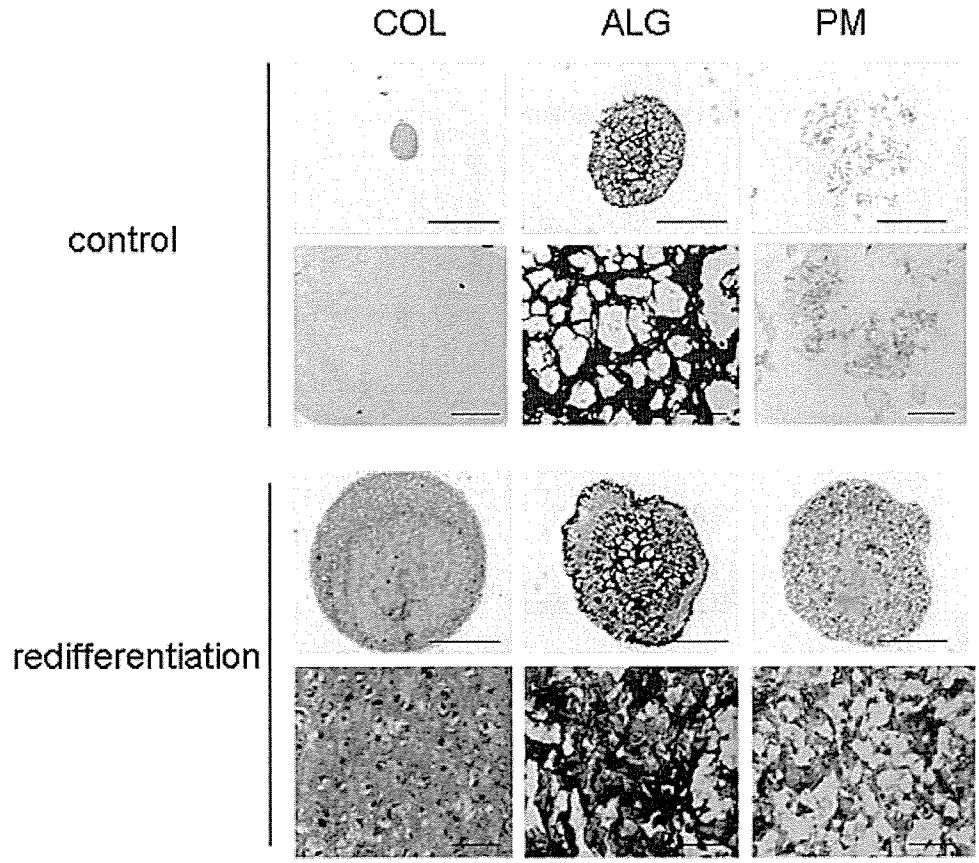

Figure 5. Histological findings for the chondrocyte/hydrogel constructs. The cell/gel constructs were metachromatically stained with toluidine blue, when they were cultured in the redifferentiation media. The internal areas of cell/PuraMatrix™ (PM) constructs showed a rather sparse and loose appearance, even in the redifferentiation medium. COL, atelopeptide collagen; ALG, alginate. Low magnification, bar = 1 mm; high = 100 μm.

the expression of β1-integrin was enhanced in high-cell density culture without any hydrogel, although it did not contain detectable amount of collagen type II and GAG. The reason why this method of culture did not accumulate cartilaginous matrices in spite of high β1-integrin expression may be that isolation of each chondrocytes was extremely diminished with cell-to-cell contacts increased, and that the 3D environment promoting chondrocyte activity could not be reproduced.

PuraMatrix™ consists of repeated sequences of RAD. The motif RAD mimics the known cell adhesion motif RGD. Actually, the RGD tripeptide of certain proteins in some species is replaced by RAD in counterparts of different species.[16] In the previous report using U251MG glioma cells, the recombinant fusion protein containing RGD promoted extensive cell attachment and spreading in cell adhesion assay, while mutation of RGD to RAD did not result in significant loss of either activity.[16] Those abundant reactive motives may also transduce the extracellular signaling into chondrocytes and induce cell growth or the gene expression of a cartilage matrix marker, such as collagen type II, in PuraMatrix™.

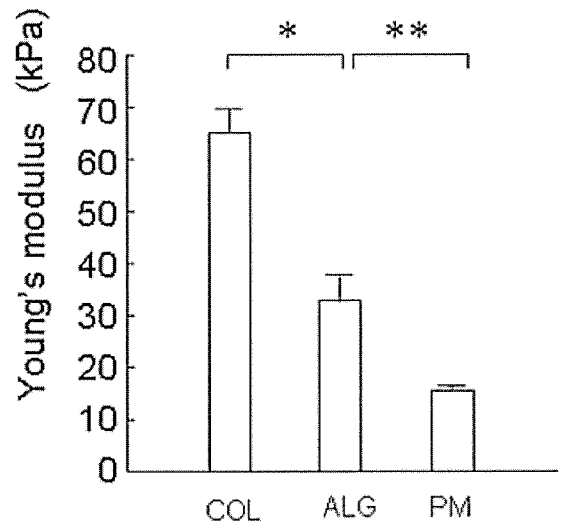

Figure 6. Young's modulus of each hydrogel. Young's modulus of each hydrogel was examined by a Venustron tactile sensor. The atelopeptide collagen showed the highest elasticity among all materials. All values are presented as mean plus standard deviation. Statistics were assessed using the Student *t* test (*: $p < 0.01$ atelopeptide collagen (COL) *vs.* alginate (ALG); **: $p < 0.01$ alginate *vs.* PuraMatrix™ (PM)).

However, the proliferation of chondrocytes or the accumulation of cartilaginous matrices, collagen type II and GAG, was rather smaller in PuraMatrix™ than in atelopeptide collagen or alginate. Histological findings also showed that the interior structure was sparse and loose in the cell/hydrogel construct using PuraMatrix™. One of the reasons was thought to be the weakness of the gelling ability and preservability for chondrocytes and matrices produced by chondrocytes within the cell/hydrogel constructs. Indeed, the gel of PuraMatrix™ showed the lowest Young's modulus among all hydrogel materials, and was soft enough to recover the cells by repeated pipetting of the cell/hydrogel construct.

On the other hand, alginate forms a firm gel. Alginate is a linear polysaccharide isolated from brown seaweed. Because it is composed of a linear co-polymer of two uronic acids, L-guluronic and D-mannuronic acid linked by β1, 4 and α1, 4 glucoside bonds,[10] it does not possess common adhesion molecules for mammalian cells. Because this kind of material hardly provides cell–matrix interactions for cells, extracellular signaling was reduced, resulting in the inhibition of chondrocyte proliferation. In contrast, a firm gel of alginate could preserve the isolation of each chondrocyte with cell-to-cell contacts decreased, as shown in Figure 3.

Cell-to-cell contacts are known to play some roles in the regulation of chondrocyte differentiation. The expression of N-cadherin in chondrocytes was changed according to the stages of differentiation. This was detectable in prechondrogenic cells, increased during cell aggregation, but became undetectable in hypertrophic chondrocytes that were embedded in abundant matrix and lost cell-to-cell contacts.[32] Also *in vitro*, N-cadherin is decreased during chondrocyte differentiation, in contrast to the upregulation of collagen type II.[33] Chondrocytes in conventional monolayer culture possess abundant cell-to-cell contacts and become dedifferentiated.[34] Also noted in the present data, the expression of N-cadherin was upregulated in the high-cell density culture without any hydrogel, suggesting an increase in cell-to-cell contacts, while the chondrocytes in this culture produced minimal amount of either collagen type II or GAG. In contrast, the 3D culture in hydrogel materials decreased the N-cadherin expression and enhanced the expression of Col2A1, even without BMP-2 and insulin. Particularly, alginate helps the chondrocytes reduce cell-to-cell contacts and maintain the cell shape and function. These properties may enhance the expression and accumulation of cartilaginous matrices such as collagen type II and GAG, in the alginate constructs.

Although alginate possesses the favorable property of inducing redifferentiation in chondrocytes and that it is widely used as a material for wound dressing on patients suffering from refractory ulcers, the application of alginate implants in the human body has not yet been clinically experienced. Because the immunoreactivity of this material during long-term intracorporeal usage has remained unknown, we should further evaluate its safety before it becomes available in clinics. On the other hand, the atelopeptide collagen has been confirmed to show even lower immunogenicity than native collagen, because telopeptides determining the antigenicity are removed from the collagen in protease digestion.[14] This kind of material has already been used to correct or repair depressed sites in soft tissue as an Atelocollagen™ implant or to compensate for a joint defect with autologous chondrocytes.[35] The atelopeptide collagen hydrogel showed some advantage for proliferation and matrix synthesis, especially collagen type II, when compared with other materials. Also in histology, the findings of cell/hydrogel constructs using the atelopeptide collagen showed abundant matrices metachromatically stained with toluidine blue, embedding round-shaped and isolated chondrocytes, which resemble physiological cartilage tissues. Therefore, the atelopeptide collagen may be accessible for clinical use in cartilage tissue engineering from the standpoints of biological properties and clinical availability.

However, the atelopeptide collagen has been prepared from animals. Although it is quality-controlled as a medical device to prevent disease transmission or to maintain a aseptic state, a discussion about the future risks for unknown disease transmission, as has been repeatedly considered for the use of FBS, may be inevitable. The use of FBS has been restricted for clinical application because it includes the risk for transmission of viral and other pathogens. Problems of a possible immune reaction against bovine protein in the serum have also been considered when the regenerated tissues cultured in the FBS-contained medium are transplanted into humans. The previous studies had shown immune response by antibody detection against bovine serum proteins in burn patients receiving keratinocyte grafts cultured from FBS.[36,37]

In Japan, the Ministry of Health, Labor and Welfare announced in 2000 that animal products from a country or zone with the occurrence of bovine spongiform encephalopathy (BSE) are prohibited for use as a medical device. According to the changes in occurrence of BSE or the policy of each nation, the supply for a medical device originating from cattle may expose the risk of arrest of supply. On this point, synthetic materials will have merits, because they may be able to control contamination or immunoreactivity. Therefore, the expectation of synthetic peptides would increase as substitutes for materials originating from organism products. Increase in gelling ability could improve supportability of cells or matrices. In the present study, we gently put the cell/PuraMatrix™ suspension into the medium adjusted to neutral pH to

form a gel. Usage of transwell dishes may induce immediate neutralization of the PuraMatrix™ and more rapid and firm gel formation, as the suppliers recommend, although we could not adopt it because we had to make uniform the experimental procedure to that of atelopeptide collagen or alginate in which the transwell dishes were not used. Some improvement of synthetic peptides would provide more useful hydrogel materials to create ideal regenerated cartilage.

References

1. Huckle J, Dootson G, Medcalf N, McTaggart S, Wright E, Carter A, Schreiber R, Kirby B, Dunkelman N, Stevenson S, Reiley S, Davisson T, Ratcliffe A. Differentiated chondrocytes for cartilage tissue engineering. Novartis Found Symp 2003; 249:103–112.
2. Kessel R. Connective Tissue: Cartilage. In: Basic Medical Histology. New York: Oxford university press; 1998. p 128–137.
3. von der Mark K, Gauss V, von der Mark H, Muller P. Relationship between cell shape and type of collagen synthesised as chondrocytes lose their cartilage phenotype in culture. Nature 1977;267:531–532.
4. Lu L, Zhu X, Valenzuela RG, Currier BL, Yaszemski MJ. Biodegradable polymer scaffolds for cartilage tissue engineering. Clin Orthop 2001(391 Suppl):S251–S270.
5. Chaipinyo K, Oakes BW, Van Damme MP. The use of debrided human articular cartilage for autologous chondrocyte implantation: Maintenance of chondrocyte differentiation and proliferation in type I collagen gels. J Orthop Res 2004;22:446–455.
6. Uchio Y, Ochi M, Matsusaki M, Kurioka H, Katsube K. Human chondrocyte proliferation and matrix synthesis cultured in Atelocollagen gel. J Biomed Mater Res 2000;50:138–143.
7. Ting V, Sims CD, Brecht LE, McCarthy JG, Kasabian AK, Connelly PR, Elisseeff J, Gittes GK, Longaker MT. In vitro prefabrication of human cartilage shapes using fibrin glue and human chondrocytes. Ann Plast Surg 1998;40:413–420.
8. Ibusuki S, Fujii Y, Iwamoto Y, Matsuda T. Tissue-engineered cartilage using an injectable and in situ gelable thermoresponsive gelatin: Fabrication and in vitro performance. Tissue Eng 2003;9:371–384.
9. Benya PD, Shaffer JD. Dedifferentiated chondrocytes reexpress the differentiated collagen phenotype when cultured in agarose gels. Cell 1982;30:215–224.
10. Stevens MM, Qanadilo HF, Langer R, Prasad Shastri V. A rapid-curing alginate gel system: Utility in periosteum-derived cartilage tissue engineering. Biomaterials 2004;25:887–894.
11. Gerard C, Catuogno C, Amargier-Huin C, Grossin L, Hubert P, Gillet P, Netter P, Dellacherie E, Payan E. The effect of alginate, hyaluronate and hyaluronate derivatives biomaterials on synthesis of non-articular chondrocyte extracellular matrix. J Mater Sci Mater Med 2005;16:541–551.
12. Malemud CJ, Stevenson S, Mehraban F, Papay RS, Purchio AF, Goldberg VM. The proteoglycan synthesis repertoire of rabbit chondrocytes maintained in type II collagen gels. Osteoarthritis Cartilage 1994;2:29–41.
13. van Susante JL, Buma P, van Osch GJ, Versleyen D, van der Kraan PM, van der Berg WB, Homminga GN. Culture of chondrocytes in alginate and collagen carrier gels. Acta Orthop Scand 1995;66:549–556.
14. Sakai D, Mochida J, Yamamoto Y, Nomura T, Okuma M, Nishimura K, Nakai T, Ando K, Hotta T. Transplantation of mesenchymal stem cells embedded in Atelocollagen gel to the intervertebral disc: A potential therapeutic model for disc degeneration. Biomaterials 2003;24:3531–3541.
15. Holmes TC, de Lacalle S, Su X, Liu G, Rich A, Zhang S. Extensive neurite outgrowth and active synapse formation on self-assembling peptide scaffolds. Proc Natl Acad Sci USA 2000;97:6728–6733.
16. Prieto AL, Edelman GM, Crossin KL. Multiple integrins mediate cell attachment to cytotactin/tenascin. Proc Natl Acad Sci USA 1993;90:10154–10158.
17. Semino CE, Merok JR, Crane GG, Panagiotakos G, Zhang S. Functional differentiation of hepatocyte-like spheroid structures from putative liver progenitor cells in three-dimensional peptide scaffolds. Differentiation 2003;71:262–270.
18. Grunder T, Gaissmaier C, Fritz J, Stoop R, Hortschansky P, Mollenhauer J, Aicher WK. Bone morphogenetic protein (BMP)-2 enhances the expression of type II collagen and aggrecan in chondrocytes embedded in alginate beads. Osteoarthritis Cartilage 2004;12:559–567.
19. Kato Y, Gospodarowicz D. Growth requirements of low-density rabbit costal chondrocyte cultures maintained in serum-free medium. J Cell Physiol 1984;120:354–363.
20. Aszodi A, Hunziker EB, Brakebusch C, Fassler R. Beta1 integrins regulate chondrocyte rotation, G1 progression, and cytokinesis. Genes Dev 2003;17:2465–2479.
21. Woodward WA, Tuan RS. N-Cadherin expression and signaling in limb mesenchymal chondrogenesis: Stimulation by poly-L-lysine. Dev Genet 1999;24:178–187.
22. Ikeda T, Kamekura S, Mabuchi A, Kou I, Seki S, Takato T, Nakamura K, Kawaguchi H, Ikegawa S, Chung UI. The combination of SOX5, SOX6, and SOX9 (the SOX trio) provides signals sufficient for induction of permanent cartilage. Arthritis Rheum 2004;50:3561–3573.
23. Franssen ME, Zeeuwen PL, Vierwinden G, van de Kerkhof PC, Schalkwijk J, van Erp PE. Phenotypical and functional differences in germinative subpopulations derived from normal and psoriatic epidermis. J Invest Dermatol 2005;124:373–383.
24. Nishida M, Kawai K, Tanaka M, Tegoshi T, Arizono N. Expression of E-cadherin in human mast cell line HMC-1. Apmis 2003;111:1067–1074.
25. Aoyagi R, Yoshida T. Frequency equations of an ultrasonic vibrator for the elastic sensor using a contact impedance method. Jpn J Appl Phys 2004;43:3204–3209.
26. Svoboda KK. Chondrocyte-matrix attachment complexes mediate survival and differentiation. Microsc Res Tech 1998;43: 111–122.
27. Hynes RO. Integrins: Bidirectional, allosteric signaling machines. Cell 2002;110:673–687.
28. Kurtis MS, Schmidt TA, Bugbee WD, Loeser RF, Sah RL. Integrin-mediated adhesion of human articular chondrocytes to cartilage. Arthritis Rheum 2003;48:110–118.
29. Grashoff C, Aszodi A, Sakai T, Hunziker EB, Fassler R. Integrin-linked kinase regulates chondrocyte shape and proliferation. EMBO Rep 2003;4:432–438.
30. Terpstra L, Prud'homme J, Arabian A, Takeda S, Karsenty G, Dedhar S, St-Arnaud R. Reduced chondrocyte proliferation and chondrodysplasia in mice lacking the integrin-linked kinase in chondrocytes. J Cell Biol 2003;162:139–148.
31. Nishihara T, Miyata T. The effects of proteases on the soluble and insoluble collagens and the structures of the insoluble collagen fiber. Collagen Symp 1962;3:66–93.
32. Tavella S, Raffo P, Tacchetti C, Cancedda R, Castagnola P. N-CAM and N-cadherin expression during in vitro chondrogenesis. Exp Cell Res 1994;215:354–362.
33. Yoon YM, Kim SJ, Oh CD, Ju JW, Song WK, Yoo YJ, Huh TL, Chun JS. Maintenance of differentiated phenotype of articular chondrocytes by protein kinase C and extracellular signal-regulated protein kinase. J Biol Chem 2002;277:8412–8420.

34. Stokes DG, Liu G, Coimbra IB, Piera-Velazquez S, Crowl RM, Jimenez SA. Assessment of the gene expression profile of differentiated and dedifferentiated human fetal chondrocytes by microarray analysis. Arthritis Rheum 2002;46:404–419.
35. Ochi M, Uchio Y, Kawasaki K, Wakitani S, Iwasa J. Transplantation of cartilage-like tissue made by tissue engineering in the treatment of cartilage defects of the knee. J Bone Joint Surg Br 2002;84:571–578.
36. Meyer AA, Manktelow A, Johnson M, deSerres S, Herzog S, Peterson HD. Antibody response to xenogeneic proteins in burned patients receiving cultured keratinocyte grafts. J Trauma 1988;28:1054–1059.
37. Johnson LF, deSerres S, Herzog SR, Peterson HD, Meyer AA. Antigenic cross-reactivity between media supplements for cultured keratinocyte grafts. J Burn Care Rehabil 1991;12: 306–312.

Available online at www.sciencedirect.com
ScienceDirect
Biochemical and Biophysical Research Communications 354 (2007) 846–851
BBRC
www.elsevier.com/locate/ybbrc

Impaired bone fracture healing in matrix metalloproteinase-13 deficient mice

Naoto Kosaki [a], Hironari Takaishi [a], Satoru Kamekura [b], Tokuhiro Kimura [c], Yasunori Okada [c], Li Minqi [d], Norio Amizuka [d], Ung-il Chung [b], Kozo Nakamura [b], Hiroshi Kawaguchi [b], Yoshiaki Toyama [a], Jeanine D'Armiento [e,*]

[a] *Department of Orthopaedic Surgery, School of Medicine, Keio University, Tokyo, Japan*
[b] *Sensory & Motor System Medicine, Faculty of Medicine, University of Tokyo, Tokyo, Japan*
[c] *Department of Pathology, School of Medicine, Keio University, Tokyo, Japan*
[d] *Center for Transdisciplinary Research, Niigata University, Niigata, Japan*
[e] *Department of Medicine, Columbia University, 630 West 168th Street, P&S 9-449 New York, NY 10032, USA*

Received 19 December 2006
Available online 19 January 2007

Abstract

Vascular and cellular invasion into the cartilage is a critical step in the fracture healing. Matrix metalloproteinase-13 (MMP-13) is a member of the zinc-dependent endopeptidase family and plays an important role in remodeling of extracellular matrix. Therefore we investigated the possible involvement of MMP-13 in a murine model of stabilized bone fracture healing. Repair of the fracture in MMP-13 deficient (MMP-13$^{-/-}$) mice was significantly delayed and characterized by a retarded cartilage resorption in the fracture callus. Immunohistochemistry indicated severe defects in vascular penetration and chondroclast recruitment to the fracture callus in MMP-13$^{-/-}$ mice. Consistent with the observations, the chondrocyte pellets cultured from the MMP13$^{-/-}$ mice exhibited diminished angiogenic activities when the pellets were co-cultured with endothelial cells. These results suggest that MMP-13 is crucial to the process of angiogenesis during healing of fracture, especially in the cartilage resorption process.

Keywords: MMP-13; Fracture healing; Extracellular matrix; Angiogenesis; Chondroclast

Bone fracture triggers a steady cascade of bone regeneration. Under optimal conditions, fractured bone heals without scar formation and fully recovers its morphological and biomechanical properties. This reparative process consists of a variety of molecular and cellular events, which recapitulate several aspects of skeletal development [1]. Although various growth factors and cytokines that participate in fracture healing have been identified [2], the precise mechanism behind these processes has not been fully elucidated.

Matrix metalloproteinases (MMPs) constitute a family of zinc-dependent proteinases which have essential roles in degradation of extracellular matrix (ECM) components such as collagens and proteoglycans. They are involved in normal development and tissue dysfunction under various pathophysiological conditions including wound healing, arthritis, and tumor development [3]. Among the members of secreted-type MMPs, MMP-9, and MMP-13 are thought to be important to normal skeletal development in mice [4–6]. MMP-13 is primarily expressed in osteoblasts and hypertrophic chondrocytes, while MMP-9 is mainly expressed in osteoclasts [7]. In contrast to the difference in their expression patterns, MMP-9 deficient (MMP-9$^{-/-}$) mice and MMP-13 deficient (MMP-13$^{-/-}$) mice exhibited similar skeletal phenotypes characterized by the elongation of hypertrophic cartilage zone in the growth plates [4–6]. The skeletal defects in MMP-9$^{-/-}$ mice are explained by

* Corresponding author.
E-mail address: jmd12@columbia.edu (J. D'Armiento).

0006-291X/$ - see front matter © 2007 Elsevier Inc. All rights reserved.
doi:10.1016/j.bbrc.2006.12.234

the impaired angiogenesis as vascular invasion of calcified cartilage is a crucial step for endochondral bone formation [8]. Because of the critical involvement of MMP-13 in endochondral bone development, we conducted the following experiments to analyze the role of MMP-13 in fracture healing.

In the current study, we generated a stabilized bone fracture at the middle of the tibia in MMP-13$^{-/-}$ mice and the healing process was then compared with those of WT mice. Cartilage formation and the angiogenic activity of chondrocytes derived from MMP-13$^{-/-}$ and WT mice were also analyzed using an *in vitro* chondrocyte culture system. The lack of MMP-13 leads to a severe delay in fracture healing, which is characterized by prolonged absorption of the fracture callus. In addition, chondrocytes derived from MMP-13$^{-/-}$ mice exhibit diminished angiogenic activity. These observations deepen our understanding of fracture healing and further underscore the importance of MMP-13 during this pathological condition.

Materials and methods

Animals. MMP-13$^{-/-}$ and WT male littermates in a C57BL/6J and 129/Sv hybrid background were generated from the intercross between heterozygous MMP-13$^{+/-}$ mice. The generation of MMP-13$^{-/-}$ mice is described elsewhere [9]. All experiments were performed according to the protocol approved by the Laboratory Animal Care and Use Committee of Keio University School of Medicine.

Fracture model. Bone fractures were generated essentially as previously described [10]. Thirty 8-week-old mice were used in each group. Briefly, under general anesthesia with xylazine (0.2 mg /10 g body weight, Bayer) and ketamine (0.5 mg/10 g body weight, Sankyo), an anterior knee incision was made, and a transverse osteotomy was performed at the middle of the tibia with a bone saw (Volvere GX, NSK Nakanishi). Fractured bones were repositioned and stabilized by inserting the inner pin of a 23-gauge spinal needle intramedullary. The mice were euthanized by cervical dislocation at designated time points and their tibiae were excised.

Radiological analysis. Bone radiographs were taken with a soft X-ray instrument (CMB-2, SOFTEX). Microarchitecture of the fracture callus was evaluated by using a micro-CT system (Scan Xmate-A100S40, Comscantecno). Calcified area and bone mineral content (BMC) of the entire tibiae were measured by a single energy X-ray absorptiometry utilizing a bone mineral analyzer for small animals (PIXImus, LUNAR), and gain of the calcified area and % gain of the BMC were calculated.

Histological analysis. The harvested tibiae were fixed in 4% paraformaldehyde, decalcified in 0.5 M EDTA (pH 7.4), embedded in paraffin, and then cut into 4-μm sections. Alcian blue and van Gieson stainings were performed according to the standard procedure. Ratio of cartilage area and bone area to total callus area was measured by a planimetric method using NIH Image.

Histochemical detection of tartrate resistant acid phosphatase (TRAP) and immunohistochemistry of type II collagen, type X collagen, MMP-9, CD31, and cathepsin K were performed as previously described [11,12].

Cell cultures. Rib chondrocytes were isolated from neonatal MMP-13$^{-/-}$ and WT littermates, and maintained in Dulbecco's modified Eagle's medium (DMEM) containing 10% fetal bovine serum and antibiotics. Human umbilical vein endothelial cells (HUVEC, Kurabo) were cultured in HuMedia-EG2 medium (Kurabo). All the cells were maintained at 37 °C in a humidified CO_2 incubator. Any chemicals if not mentioned otherwise were purchased from Sigma.

Cell differentiation assay. To induce chondrogenic differentiation, chondrocyte 3D culture was performed as previously described [13]. Briefly, chondrocytes were suspended in atelopeptide collagen solution (0.5% atelopeptide collagen (Kawaken Fine Chemicals)/5 mM NaOH/26 mM $NaHCO_3$/20 mM Hepes/one volume of 10 times concentrated α-minimal essential medium (αMEM)) at a density of 1×10^7 cells/ml. Each 20 μl of the mixture was placed into the bottom of 15 ml conical tubes (Falcon) and incubated for 1 h at 37 °C to form a gel. DMEM with 200 ng/ml recombinant human bone morphogenetic protein-2 (kindly provided by Astellas Pharma Inc.), 5 μg/ml insulin and antibiotics (chondrogenic medium) was gently poured onto the gel at a volume of 1 ml. The paraffin sections of the pellets were made after fixation with 4% paraformaldehyde and stained with Alcian blue.

Angiogenesis assay. For the *in vitro* angiogenesis assay, the chondrocyte pellets that had been cultured in chondrogenic medium for 3 weeks were co-cultured with HUVEC. HUVEC were suspended in a collagen gel solution (Cellmatrix type IA (Nitta Gelatin)/5 mM NaOH/26 mM $NaHCO_3$/20 mM Hepes/one volume of 10 times concentrated αMEM) at a density of 1×10^6 cells/ml, and 400 μl of the mixture was poured into each well of 24-well plates. The chondrocyte pellets were then dropped at the center of each well and incubated for 30 min at 37 °C to form a gel. These cells were cultured together in HuMedia-EG2 medium and the angiogenic reactions were monitored for 2 weeks.

Statistical analysis. Means of groups were compared by analysis of variance, and significance of differences was determined by post hoc testing using Bonferroni's method.

Results

MMP-13$^{-/-}$ mice exhibit delayed fracture healing

To investigate the effect of MMP-13 on fracture healing, we generated a stabilized tibial fracture model in mice and assessed the healing process by radiological evaluation (Fig. 1A). In plain radiographs of WT mice, the calcified callus appeared at post-fracture week (PFW) 1, progressed to form a bony bridge by PFW3, and then gradually decreased in size by PFW10. In contrast, in the MMP-13$^{-/-}$ mice, a radiolucent zone was apparent in the fracture callus even at PFW3, suggesting that with the loss of MMP-13 the bony bridging was delayed. In axial CT images, the WT mouse callus contained a small noncalcified area at PFW2, which was subsequently replaced by calcification at PFW3. However, in MMP-13$^{-/-}$ mice, the callus consisted mainly of noncalcified tissue at PFW2, and although calcification progressed, there remained an area of noncalcified tissue at PFW3.

To quantify the extent of callus formation, the calcified area and BMC in the fractured and control tibiae were measured by a bone densitometer. As shown in Fig. 1B, both parameters increased for 3 weeks during the modeling phase and then decreased during the remodeling phase in WT mice. In contrast, MMP-13$^{-/-}$ mice showed a significant reduction in these parameters at PFW2-3 during the modeling phase. There were no differences in the calcified area and BMC between the two genotypes during the remodeling phase (PFW4-10). These results indicate that MMP-13 deficiency causes a delay in fracture healing through impaired bone modeling due to retarded calcification of the fracture callus.

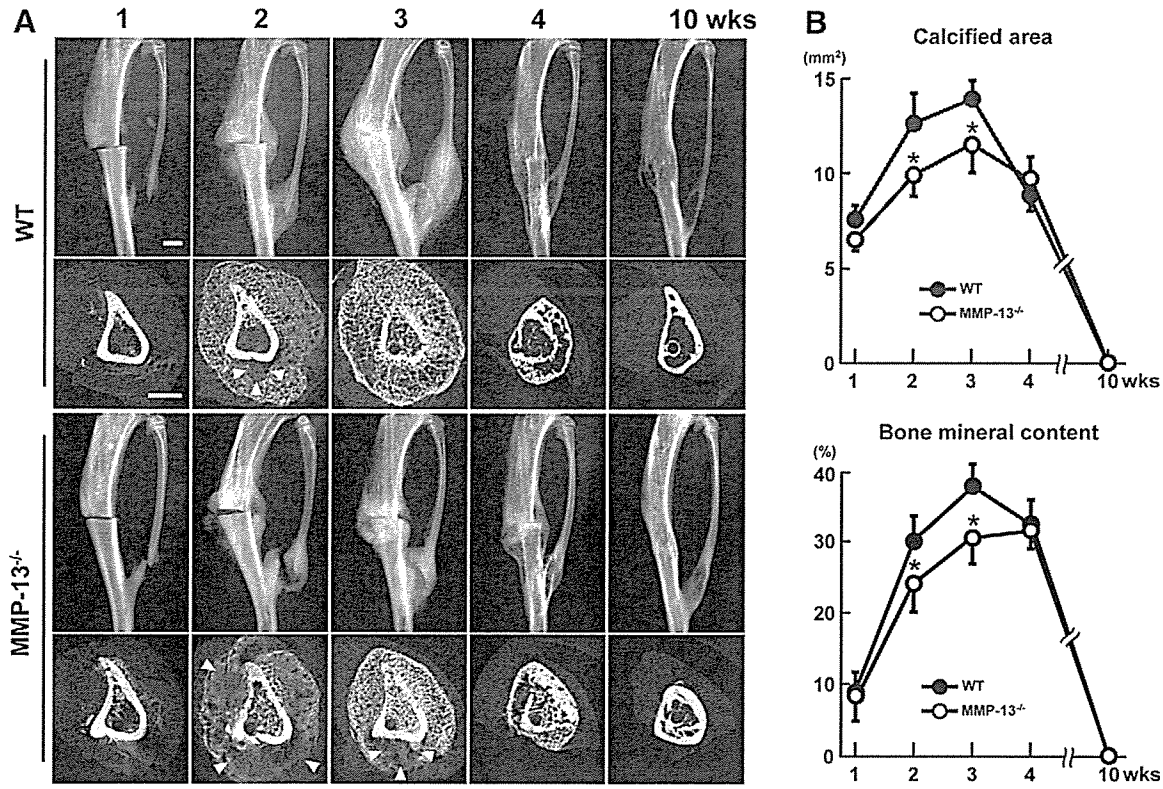

Fig. 1. Radiological analyses of bone fracture healing in WT and MMP-13$^{-/-}$ mice. (A) Plain radiographs (upper row) and CT images (lower row) of the representative fractured tibiae in WT and MMP-13$^{-/-}$ mice at PFWs 1–10. The arrowheads indicate non-calcified areas. Scale bar, 1 mm. (B) Time course changes of the calcified area and bone mineral content of the callus at the fracture site measured by single energy X-ray absorptiometry. Data are expressed as the means (symbols) ± SD (error bars) of 6 mice per genotype. $^{*}p < 0.05$ versus WT.

MMP-13 deficiency impairs the replacement of cartilage with bone in the fracture callus

Remodeling of bone requires the resorption of cartilage, which provides initial stabilization to the fractured bone [2]. To evaluate the turnover of cartilage to bone in the fracture callus, the ratio of cartilage area and bone area to total callus area (CA/TA and BA/TA, respectively) were measured utilizing a planimetric method in histological sections (Fig. 2). The cartilage area was stained blue with Alcian blue staining, and the bone area was stained red with van Gieson. In WT mice, CA/TA reached its peak value at PFW1 and then decreased by PFW4, whereas BA/CA increased to reach a plateau by PFW3. Compared to WT mice, MMP-13$^{-/-}$ mice exhibited higher CA/TA values and lower BA/TA values at PFW2-3, indicating that loss of MMP-13 interferes with cartilage-to-bone replacement.

MMP-13 deficiency impairs vascular and chondroclast invasion of cartilage

To further investigate the mechanisms underlying the impaired bone healing in MMP-13$^{-/-}$ mice, we performed immunohistochemical analysis of the fracture callus at PFW2 (Fig. 3). Type X collagen, a marker for hypertrophic chondrocytes, was more prevalent in the MMP-13$^{-/-}$ cartilage than in the WT cartilage, while type II collagen was equivalent between the genotypes (Fig. 3A–D). MMP-9 was expressed in hypertrophic chondrocytes and chondroclasts, and appeared to be up-regulated in the MMP-13$^{-/-}$ mice (Fig. 3E and F). In WT mice, the CD31-immunostained capillaries penetrated into the cartilage extending their cytoplasmic processes (Fig. 3G), and cathepsin K/TRAP-positive chondroclasts were directly attached to the cartilage matrix (Fig. 3I and K). In contrast, MMP-13$^{-/-}$ mice showed minimal cartilaginous breakage associated with capillary invasion (Fig. 3H), and the chondroclasts were not attached to the cartilage matrix (Fig. 3J and L). These findings suggest that the impaired cartilage resorption in the MMP-13$^{-/-}$ mouse callus is associated with the inability of capillaries and chondroclasts to invade the cartilage.

MMP-13 is required for the angiogenic activation of cartilage

In order to clarify the cellular mechanism underlying these abnormalities, we examined *in vitro* the differentiation of rib chondrocytes isolated from WT and MMP-13$^{-/-}$ littermates (Fig. 4). Calvarial osteoblasts cultured from MMP-13$^{-/-}$ mice exhibited no difference in proliferation and differentiation compared with those from WT mice,

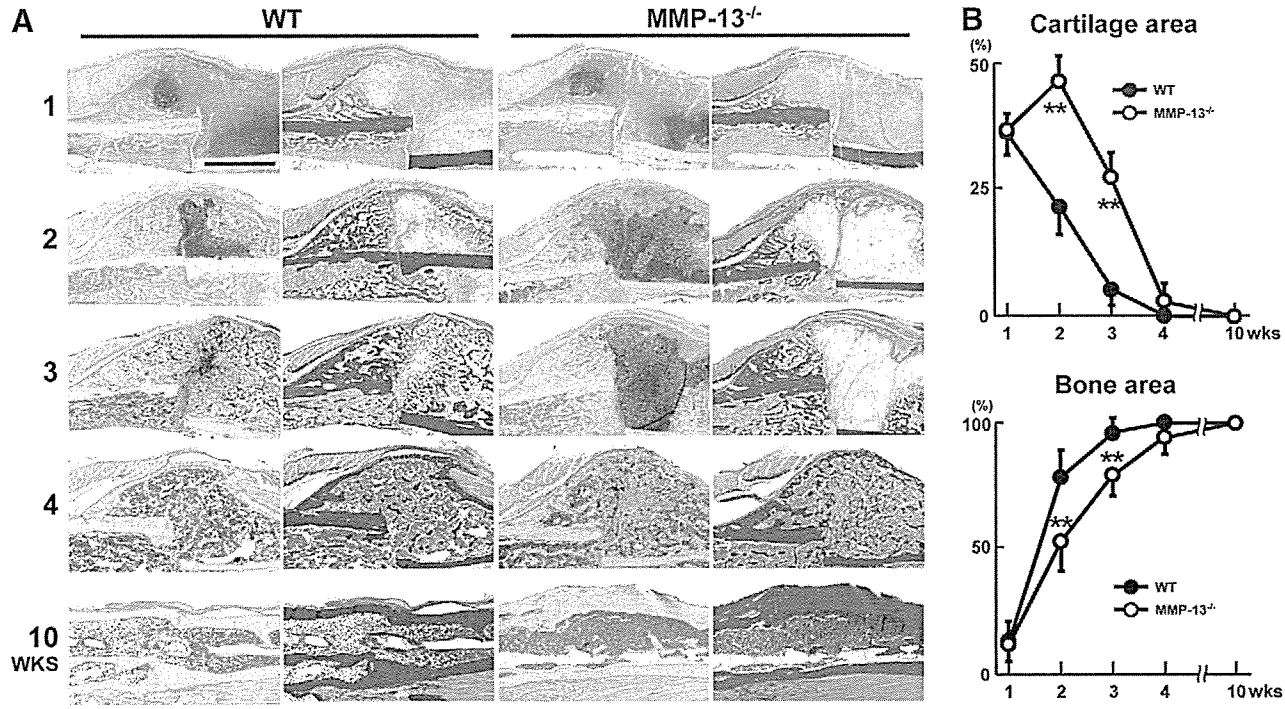

Fig. 2. Histomorphological analyses of bone fracture healing in WT and MMP-13$^{-/-}$ mice. (A) Alcian blue staining (right column) and van Gieson staining (left column) of the fractured tibia sections from WT and MMP-13$^{-/-}$ mice. Scale bar, 1 mm. (B) Ratios of cartilage area and bone area to total callus area of the fractured site, which were measured by a planimetric method. Data are expressed as the means (symbols) ± SD (error bars) of 6 mice per genotype. $^{**}p < 0.01$ versus WT.

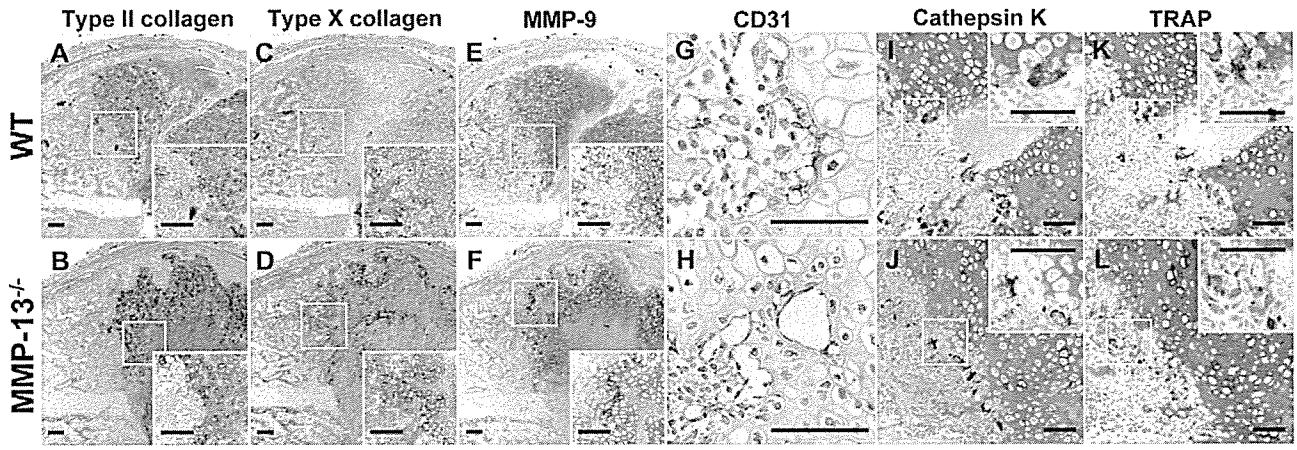

Fig. 3. Immunohistochemical and histochemical analyses of bone fracture healing in WT and MMP-13$^{-/-}$ mice. (A–J) Immunohistochemistry of type II collagen (A,B), type X collagen (C,D), MMP-9 (E,F), CD31 (G,H) and cathepsin K (I,J) in the fracture callus of WT and MMP-13$^{-/-}$ mice at PFW2. (K,L) Histochemistry for TRAP in the fracture callus of WT and MMP-13$^{-/-}$ mice at PFW2. All insets are higher magnification images of each figure. Note that the expression of type X collagen and MMP-9 in hypertrophic chondrocytes and/or chondroclasts appear to be up-regulated in MMP-13$^{-/-}$ mice compared to WT mice (C–F). Also note that and cathepsin K/TRAP-positive chondroclasts are unattached to cartilage matrix in MMP-13$^{-/-}$ mice (J,L). Scale bar, 80 μm.

and the cell proliferation rate of MMP-13$^{-/-}$ chondrocytes was also normal (data not shown).

To evaluate the cartilage formation, chondrocytes were cultured in 3D collagen gel pellets. During the first 2 days the WT pellets shrunk and the cartilage matrix formation by the chondrocytes was observed at the pellet periphery on day 7. By 21 days cartilage maturation proceeded toward the center forming a mature cartilage pellet. In the MMP-13$^{-/-}$ pellets, the gel contraction rate on day 2 and matrix synthesis on day 7 were reduced compared to WT pellets, although the matured pellets exhibited no histological differences between genotypes on day 21.

To further investigate the angiogenic property of the cartilage pellets, we developed a co-culture system of the chondrocyte pellets with HUVEC. After 1 week of co-culture, extensive vascular sprouting was observed around the

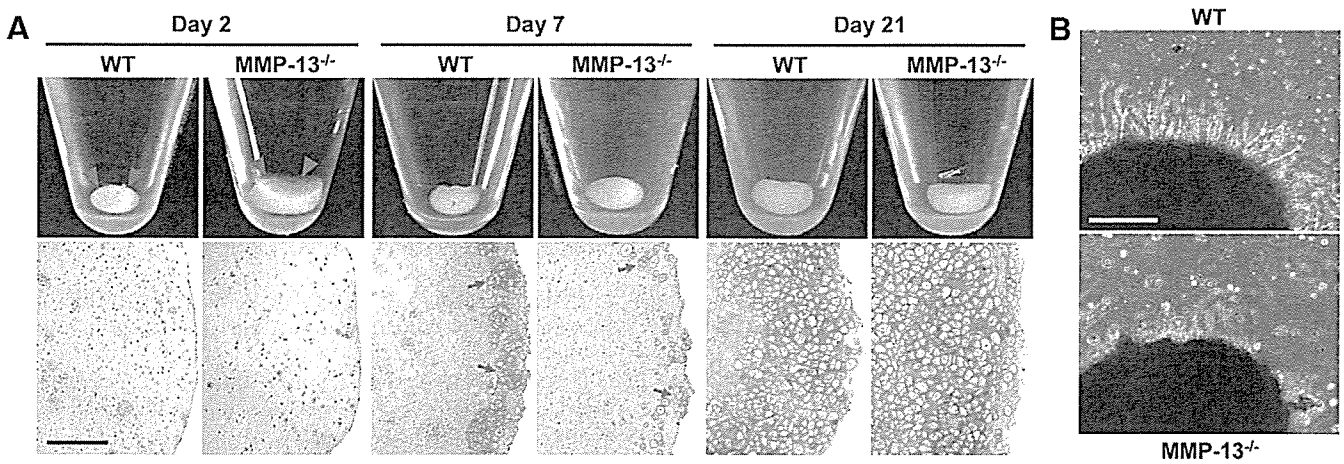

Fig. 4. Cultured chondrocytes from WT and MMP-13$^{-/-}$ mice. (A) Gross appearance (upper row) and Alcian blue stainings (lower row) of chondrocyte pellets on days 2, 7, and 21. Chondrocytes from WT and MMP-13$^{-/-}$ mice were cultured in 3D collagen gel pellets. Note that MMP-13$^{-/-}$ pellet is reduced in gel contraction rate on day 2 (arrowheads) and Alcian blue-positive matrix synthesis on day 7 (arrows). Scale bar, 500 μm. (B) *In vitro* angiogenesis assay. Chondrocyte pellets were co-cultured with HUVEC in collagen gel. Note that WT pellets are surrounded by numerous vascular sproutings, which are barely seen with the MMP-13$^{-/-}$ pellets. Scale bar, 250 μm.

WT pellets, although the MMP-13$^{-/-}$ pellets exhibited limited sprouting (Fig. 4B). These results suggest that MMP-13 is involved in the angiogenic activation of chondrocytes via matrix remodeling.

Discussion

MMP-13 is the major proteinase that cleaves interstitial fibrillar collagens (type I, II, and III collagens) [14]. Deficiency of MMP-13 causes a transient elongation of the hypertrophic zone in the growth plate during the early stages of growth and development, indicating a role for this enzyme in endochondral bone development [5,6]. Since the bone fracture healing process is thought to recapitulate skeletal development [1], and since MMP-13 is highly expressed in the fracture callus [7], we hypothesized that MMP-13 plays an important role in fracture healing. Utilizing a mouse fracture model and a chondrocyte pellet culture, the present studies demonstrate that the lack of MMP-13 leads to a significant delay in the fracture healing process, and that MMP-13 plays a critical role in the maturation of chondrocytes and the induction of angiogenesis.

During the bone fracture healing process, fracture callus consisting of cartilage tissue is transiently formed and subsequently resorbed and replaced with osseous tissue; hence the cartilage resorption process is an important step for fracture healing. In general, the vascular invasion is a critical rate-limiting determinant for bone formation [15], and at the chondroosseous junction there are three key players in this process: hypertrophic chondrocytes, capillaries, and chondroclasts [16]. Among them, hypertrophic chondrocytes are the major cell type producing MMP-13 in the fracture callus and, in MMP-13$^{-/-}$ mice, the cartilage resorption was delayed due to the impairment of the invasion of capillaries and chondroclasts into the cartilage. These data re-emphasize the role of vascular and chondroclast invasion during the fracture callus resorption and indicate that MMP-13 production by chondrocytes is a prerequisite for this process.

Since primary chondrocytes from the rib cartilage were not capable of effectively producing ECM in a monolayer culture, we utilized a 3D pellet culture model to mimic the *in vivo* environment. Cells/collagen gel composites are known to undergo shrinkage during culture [17], and early gel contraction and subsequent matrix synthesis in the MMP-13$^{-/-}$ chondrocyte pellets were both suppressed compared to those observed in WT controls, suggesting that cell–ECM and/or cell–cell interactions caused by gel contraction are important for chondrocyte development and that MMP-13 is involved in these processes. These findings are similar to those seen in mice deficient in α1 integrin, a key molecule for cell–ECM interaction, which exhibited reduced cartilage ECM synthesis during fracture healing [18]. Moreover, interactions of chondrocytes with their ECM are required for the expression of angiogenic activities of chondrocytes [19]. When chondrocyte pellets and endothelial cells from the MMP-13$^{-/-}$ mice were co-cultured, tubular formation was considerably reduced in the pellets from MMP-13$^{-/-}$ mice, indicating that MMP-13 is critical for the angiogenic activities of chondrocytes. These data strongly support the notion that MMP-13 contributes to the fracture healing process by regulating both chondrocyte development and vascular induction.

MMP-9 deficiency has been shown to cause delayed fracture healing [8] in a manner similar to that seen in the MMP-13$^{-/-}$ mice. MMP-9$^{-/-}$ mice exhibit hindered cartilage resorption mainly due to suppressed angiogenesis, which can be rescued by local injection of recombinant vascular endothelial growth factor. Similar to the MMP-13$^{-/-}$ mice, elongation of the hypertrophic cartilage zone is also observed in the MMP-9$^{-/-}$ mice [4–6], although the expression pattern of these enzymes are different; in bone tissue MMP-9 is expressed mainly in osteoclasts and chondroclasts while MMP-13 is expressed mainly in osteoblasts

and chondrocytes [7]. In line with the findings of the growth plates of MMP-13$^{-/-}$ mice in which MMP-9 mRNA expression is up-regulated [5], the intensity of MMP-9 expression in the fracture callus was higher in MMP-13$^{-/-}$ mice compared to that in WT mice. These findings indicate a possible compensatory/redundant mechanism between these two MMPs during cartilage resorption in both physiological and pathological conditions, where chondrocytes, endothelial cells, and chondroclasts are intricately regulated.

In conclusion, the current study provides *in vivo* and *in vitro* evidence for the critical role of MMP-13 in cartilage resorption during bone fracture healing. In addition, the finding that MMP-13 plays a major role in vascular invasion of cartilage provides an incentive to further study the mechanism underlying the pro-angiogenic function of MMP-13. Moreover, it will be interesting to examine the compensatory role of MMPs, such as MMP-9 and MMP-13, in fracture healing. Taken together, this study provides new insight into the role of MMP-13 in fracture healing, which in turn has implications for bone regenerative medicine.

Acknowledgments

The authors thank Dr. K. Horiuchi and Dr. J. Takito for critical discussions. We are grateful to Dr. K. Hoshi for sharing his expertise on the chondrocyte culture system. This study was supported by the National Institute of Aging (AG016994) and the Grants-in-Aid provided by the Ministry of Education, Science and Culture, Japan for General Scientific Research and Scientific Research on Priority Areas; by the Uehara Foundation and the General Insurance Association of Japan.

References

[1] L.C. Gerstenfeld, D.M. Cullinane, G.L. Barnes, D.T. Graves, T.A. Einhorn, Fracture healing as a post-natal developmental process: molecular, spatial, and temporal aspects of its regulation, J. Cell. Biochem. 88 (2003) 873–884.

[2] G.L. Barnes, P.J. Kostenuik, L.C. Gerstenfeld, T.A. Einhorn, Growth factor regulation of fracture repair, J. Bone Miner. Res. 14 (1999) 1805–1815.

[3] J.M. Milner, T.E. Cawston, Matrix metalloproteinase knockout studies and the potential use of matrix metalloproteinase inhibitors in the rheumatic diseases, Curr. Drug Targets Inflamm. Allergy 4 (2005) 363–375.

[4] T.H. Vu, J.M. Shipley, G. Bergers, J.E. Berger, J.A. Helms, D. Hanahan, S.D. Shapiro, R.M. Senior, Z. Werb, MMP-9/gelatinase B is a key regulator of growth plate angiogenesis and apoptosis of hypertrophic chondrocytes, Cell 93 (1998) 411–422.

[5] M. Inada, Y. Wang, M.H. Byrne, M.U. Rahman, C. Miyaura, C. Lopez-Otin, S.M. Krane, Critical roles for collagenase-3 (Mmp13) in development of growth plate cartilage and in endochondral ossification, Proc. Natl. Acad. Sci. USA 101 (2004) 17192–17197.

[6] D. Stickens, D.J. Behonick, N. Ortega, B. Heyer, B. Hartenstein, Y. Yu, A.J. Fosang, M. Schorpp-Kistner, P. Angel, Z. Werb, Altered endochondral bone development in matrix metalloproteinase 13-deficient mice, Development 131 (2004) 5883–5895.

[7] H. Uusitalo, A. Hiltunen, M. Soderstrom, H.T. Aro, E. Vuorio, Expression of cathepsins B, H, K, L, and S and matrix metalloproteinases 9 and 13 during chondrocyte hypertrophy and endochondral ossification in mouse fracture callus, Calcif. Tissue Int. 67 (2000) 382–390.

[8] C. Colnot, Z. Thompson, T. Miclau, Z. Werb, J.A. Helms, Altered fracture repair in the absence of MMP9, Development 130 (2003) 4123–4133.

[9] H. Takaishi, T. Kimura, S. Dalal, Y. Okada, J. D'Armiento, Joint diseases and matrix metalloproteinases: a role for MMP-13, Curr. Pharma. Biotechnol. (2007) in press.

[10] T. Shimoaka, S. Kamekura, H. Chikuda, K. Hoshi, U.I. Chung, T. Akune, Z. Maruyama, T. Komori, M. Matsumoto, W. Ogawa, Y. Terauchi, T. Kadowaki, K. Nakamura, H. Kawaguchi, Impairment of bone healing by insulin receptor substrate-1 deficiency, J. Biol. Chem. 279 (2004) 15314–15322.

[11] M. Li, N. Amizuka, K. Takeuchi, P.H. Freitas, Y. Kawano, M. Hoshino, K. Oda, K. Nozawa-Inoue, T. Maeda, Histochemical evidence of osteoclastic degradation of extracellular matrix in osteolytic metastasis originating from human lung small carcinoma (SBC-5) cells, Microsc. Res. Tech. 69 (2006) 73–83.

[12] N. Amizuka, D. Davidson, H. Liu, G. Valverde-Franco, S. Chai, T. Maeda, H. Ozawa, V. Hammond, D.M. Ornitz, D. Goltzman, J.E. Henderson, Signalling by fibroblast growth factor receptor 3 and parathyroid hormone-related peptide coordinate cartilage and bone development, Bone 34 (2004) 13–25.

[13] H. Yamaoka, H. Asato, T. Ogasawara, S. Nishizawa, T. Takahashi, T. Nakatsuka, I. Koshima, K. Nakamura, H. Kawaguchi, U.I. Chung, T. Takato, K. Hoshi, Cartilage tissue engineering using human auricular chondrocytes embedded in different hydrogel materials, J. Biomed. Mater Res. A 78 (2006) 1–11.

[14] B. Lovejoy, A.R. Welch, S. Carr, C. Luong, C. Broka, R.T. Hendricks, J.A. Campbell, K.A. Walker, R. Martin, H. Van Wart, M.F. Browner, Crystal structures of MMP-1 and -13 reveal the structural basis for selectivity of collagenase inhibitors, Nat. Struct. Biol. 6 (1999) 217–221.

[15] H. Peng, A. Usas, A. Olshanski, A.M. Ho, B. Gearhart, G.M. Cooper, J. Huard, VEGF improves, whereas sFlt1 inhibits, BMP2-induced bone formation and bone healing through modulation of angiogenesis, J. Bone Miner. Res. 20 (2005) 2017–2027.

[16] R.K. Schenk, D. Spiro, J. Wiener, Cartilage resorption in the tibial epiphyseal plate of growing rats, J. Cell Biol. 34 (1967) 275–291.

[17] A. Yokoyama, I. Sekiya, K. Miyazaki, S. Ichinose, Y. Hata, T. Muneta, In vitro cartilage formation of composites of synovium-derived mesenchymal stem cells with collagen gel, Cell Tissue Res. 322 (2005) 289–298.

[18] E. Ekholm, K.D. Hankenson, H. Uusitalo, A. Hiltunen, H. Gardner, J. Heino, R. Penttinen, Diminished callus size and cartilage synthesis in alpha 1 beta 1 integrin-deficient mice during bone fracture healing, Am. J. Pathol. 160 (2002) 1779–1785.

[19] F. Descalzi Cancedda, A. Melchiori, R. Benelli, C. Gentili, L. Masiello, G. Campanile, R. Cancedda, A. Albini, Production of angiogenesis inhibitors and stimulators is modulated by cultured growth plate chondrocytes during in vitro differentiation: dependence on extracellular matrix assembly, Eur. J. Cell Biol. 66 (1995) 60–68.

JOURNAL OF BONE AND MINERAL RESEARCH
Volume 21, Number 2, 2006
Published online on November 7, 2005; doi: 10.1359/JBMR.051025

Suppression of Adjuvant-Induced Arthritic Bone Destruction by Cyclooxygenase-2 Selective Agents With and Without Inhibitory Potency Against Carbonic Anhydrase II

Mika Katagiri,[1] Toru Ogasawara,[1] Kazuto Hoshi,[1] Daichi Chikazu,[1] Aishi Kimoto,[2] Masahiro Noguchi,[2] Masao Sasamata,[2] Shun-ichi Harada,[3] Hideto Akama,[4] Hatsue Tazaki,[5] Ung-il Chung,[1] Tsuyoshi Takato,[1] Kozo Nakamura,[1] and Hiroshi Kawaguchi[1]

ABSTRACT: In vitro assays revealed that COX-2 inhibitors with CA II inhibitory potency suppressed both differentiation and activity of osteoclasts, whereas that without the potency reduced only osteoclast differentiation. However, all COX-2 inhibitors similarly suppressed bone destruction in adjuvant-induced arthritic rats, indicating that suppression of osteoclast differentiation is more effective than that of osteoclast activity for the treatment.

Introduction: Cyclooxygenase (COX)-2 and carbonic anhydrase II (CA II) are known to play important roles in the differentiation of osteoclasts and the activity of mature osteoclasts, respectively. Because several COX-2 selective agents were recently found to possess an inhibitory potency against CA II, this study compared the bone sparing effects of COX-2 selective agents with and without the CA II inhibitory potency.
Materials and Methods: Osteoclast differentiation was determined by the mouse co-culture system of osteoblasts and bone marrow cells, and mature osteoclast activity was measured by the pit area on a dentine slice resorbed by osteoclasts generated and isolated from bone marrow cells. In vivo effects on arthritic bone destruction were determined by radiological and histological analyses of hind-paws of adjuvant-induced arthritic (AIA) rats.
Results: CA II was expressed predominantly in mature osteoclasts, but not in the precursors. CA II activity was inhibited by sulfonamide-type COX-2 selective agents celecoxib and JTE-522 similarly to a CA II inhibitor acetazolamide, but not by a methylsulfone-type COX-2 inhibitor rofecoxib. In vitro assays clearly revealed that celecoxib and JTE-522 suppressed both differentiation and activity of osteoclasts, whereas rofecoxib and acetazolamide suppressed only osteoclast differentiation and activation, respectively. However, bone destruction in AIA rats was potently and similarly suppressed by all COX-2 selective agents whether with or without CA II inhibitory potency, although only moderately by acetazolamide.
Conclusions: Suppression of osteoclast differentiation by COX-2 inhibition is more effective than suppression of mature osteoclast activity by CA II inhibition for the treatment of arthritic bone destruction.
J Bone Miner Res 2006;21:219–227. Published online on November 7, 2005; doi: 10.1359/JBMR.051025

Key words: cyclooxygenase, prostaglandin, carbonic anhydrase, osteoclast, bone resorption, arthritis

INTRODUCTION

BONE DESTRUCTION CAUSING joint deformities is one of the most serious problems in patients with rheumatoid arthritis (RA). Histological analyses have shown that osteoclastic bone resorption at the bone-pannus interface plays a pivotal role in the RA bone destruction.[1] Among pro-inflammatory cytokines that play pivotal roles in the RA pathogenesis, fibroblast growth factor 2 (FGF-2) is reported to be strongly associated with osteoclastic bone resorption by RA in animal models and clinical settings.[2–4] Osteoclastic bone resorption is regulated mainly by two consecutive steps: the differentiation of osteoclasts from hemopoietic precursors and the activity of mature osteoclasts to resorb bone.

The differentiation of osteoclasts is stimulated by a variety of cytokines and hormones including FGF-2, a large part of which is mediated by the production of prostaglandins (PGs).[5] PGs stimulate osteoclast differentiation through the induction of RANKL in osteoblastic cells,[6] whereas they inhibit the bone resorptive activity of mature osteoclasts.[7] Among the synthetic enzymes of PGs, we

The authors have no conflict of interest.

[1]Sensory & Motor System Medicine, Faculty of Medicine, University of Tokyo, Bunkyo, Tokyo, Japan; [2]Drug Discovery Research, Astellas Pharma, Inc., Tsukuba, Ibaraki, Japan; [3]Department of Bone Biology and Osteoporosis Research, Merck Research Laboratories, West Point, Pennsylvania, USA; [4]Medical Division, Pfizer Japan Inc., Shibuya, Tokyo, Japan; [5]Central Pharmaceutical Research Institute, Japan Tobacco Inc., Takatsuki, Osaka, Japan.

and others have reported that cyclooxygenase-2 (COX-2) plays a central role in the biosynthesis of PGs in response to bone resorptive stimuli by cytokines and hormones,[8–12] so that COX-2 induction is involved in bone resorptive disorders including RA by inducing osteoclast differentiation.[2,13,14]

Although little is known about the direct signaling to activate mature osteoclasts, a study of random sequence analysis of PCR-amplified cDNA clones detected 14 distinct kinase-related genes in purified mature osteoclasts, and 8 of them were identified as receptor tyrosine kinases (RTKs).[15] RTKs expressed on mature osteoclasts include FGF receptor type 1 (FGFR1) and Tyro 3, whose ligands FGF-2 and the growth arrest-specific gene 6 (Gas6), respectively, are known to be potent bone resorptive cytokines. We previously reported that FGF-2 at physiological concentrations (≥10 pM) acts directly on mature osteoclasts to resorb bone by activating FGFR1,[16] whereas at higher concentrations (≥10 nM), it stimulates osteoclast differentiation by inducing RANKL mainly through COX-2 expression in osteoblasts.[10,11] In the meantime, Gas6, although ubiquitously expressed in bone cells, did not affect the osteoclast differentiation, but potently stimulated the mature osteoclast activity because of the restricted localization of its receptor Tyro 3 on mature osteoclasts.[15,17] Under these stimuli, osteoclasts resorb bone by attaching to the surface and secreting protons in an extracellular compartment formed between osteoclast and the bone surface.[18] This secretion is necessary for bone mineral solubilization and the digestion of organic bone matrix by acid proteases. For this process, carbonic anhydrase II (CA II), which is abundant in the osteoclast cytoplasm and on the inner surface of its ruffled border, catalyzes the hydration of CO_2 to bicarbonate and a proton, thereby contributing to the H^+ secretion acidifying the bone resorption compartment and to HCO_3^- secretion by the HCO_3^-/Cl^- exchanger, which maintains pH homeostasis.[19] The blockage of CA II with antisense oligonucleotides or acetazolamide, a potent CA II inhibitor, has been reported to suppress bone resorption by osteoclasts,[20,21] and a CA II deficiency syndrome has been shown to exhibit nonfunctional osteoclasts and osteopetrosis.[22] In addition, CA II expression is stronger in actively resorbing mature osteoclasts than in nonresorbing osteoclasts.[23] All these findings strongly suggest that CA II plays an important role in the bone resorptive activity of mature osteoclasts.

Interestingly, a recent report revealed that sulfonamide-type COX-2 inhibitors that contain an aryl sulfonamide moiety, such as celecoxib, show an unexpected nanomolar affinity to and inhibition of the totally unrelated carbonic anhydrase family including CA II, whereas methylsulfone-type COX-2 inhibitors without the sulfonamide moiety, such as rofecoxib, do not.[24] Hence, to investigate the importance of the regulation of osteoclast differentiation by COX-2 and osteoclast activity by CA II in arthritic bone destruction, this study examined the suppressive effects of COX-2 selective agents with and without inhibitory potency against CA II both in vivo and in vitro. For the in vitro analyses, we initially examined the stimulatory effects of FGF-2 and Gas6 on the formation of osteoclasts in the co-culture of mouse osteoblasts and bone marrow cells and on the activity of mature osteoclasts generated and isolated from osteoclast precursor macrophage colony-stimulating factor (M-CSF)–dependent bone marrow macrophages (M-BMMϕs). Suppressions of osteoclast differentiation and activation in these cultures by celecoxib, rofecoxib, JTE-522, and acetazolamide, which show distinct inhibitions on COX-2 and CA II, were examined. For the in vivo analyses, suppressions of inflammation and bone destruction of hindpaws of adjuvant-induced arthritic (AIA) rats as a model of RA by administration of these inhibitors were studied.

MATERIALS AND METHODS

Animals and materials

Eight-week-old ddY mice and 6-week-old male Lewis rats were purchased from Charles River Japan Laboratories (Kanagawa, Japan). All animal experiments were performed according to the guidelines of the International Association for the Study of Pain.[25] In addition, the experimental work was reviewed by the committee of Tokyo University charged with confirming ethics.

Celecoxib and a COX-1 selective inhibitor SC-560 were generously provided by Pfizer (New York, NY, USA). Rofecoxib was provided by Merck Sharp & Dohme (Rahway, NJ, USA) and JTE-522, a novel sulfonamide-type COX-2 selective agent,[26] was synthesized and provided by Japan Tobacco (Osaka, Japan). Rat recombinant Gas6 and human recombinant FGF-2 were generously provided by Shionogi Research Laboratory (Osaka, Japan) and Kaken Pharmaceutical Co. (Kyoto, Japan), respectively. α-MEM was purchased from Life Technologies (Grand Island, NY, USA), and FBS was from the Cell Culture Laboratory (Cleveland, OH, USA). Recombinant human M-CSF was purchased from R&D Systems (Minneapolis, MN, USA). Recombinant human soluble RANKL was purchased from PeproTech (London, UK). Bacterial collagenase and ISOGEN were purchased from Wako Pure Chemicals Co. (Osaka, Japan), and dispase from Nitta Gelatin Co. (Osaka, Japan). Other chemicals were obtained from Sigma Chemical Co. (St Louis, MO, USA), unless otherwise specified.

RT-PCR for COX-2 and CA II expression

For the osteoclast precursor cells, we used the M-BMMϕ culture described previously.[27] Briefly, bone marrow cells from tibias of 8-week-old mice were seeded at a density of 2×10^5 cells/well in 6-well dishes and cultured in α-MEM containing 10% FBS with M-CSF (100 ng/ml). After culturing for 3 days, nonadherent cells were washed with PBS, and adherent cells (M-BMMϕs) were further cultured with soluble RANKL (30 ng/ml) and M-CSF (10 ng/ml). Total RNA was extracted from the cells cultured for 1–5 days, using ISOGEN following the manufacturer's instructions, and 2 μg of RNA was reverse transcribed and amplified by PCR using the RT-PCR kit (Takara Biomedicals, Shiga, Japan). The primers were as follows: sense, 5′-TCAGCCAGGCAGCAAATCCTTG-3′ and antisense, 5′-TAGTCTCTCCTATGAGTATGAGTC-3′ for COX-2; sense, 5′-CTCTCAGGACAATGCAGTGC-3′ and anti-

sense, 5′-ATCCAGGTCACACATTCCAGC-3′ for CA II; and 5′-CATGTAGGCCATGAGGTCCACCAC-3′ and 5′-TGAAGGTCGGTGTGAACGGATTTGGC-3′ G3PDH. The cycling parameters were 45 s at 94°C, 30 s at 56°C, and 90 s at 72°C for 26 cycles.

CA II activity

The inhibitory effects of COX-2 inhibitors and acetazolamide, a positive control, on CA II activity was determined by the method reported by Wilbur et al.[28] Briefly, the Universal buffer (25 mM; lot 01020; Helena Laboratories, Beaumort, TX, USA) with or without CA II (100 Wilbur-Andersone units/ml; Sigma) at pH 8.6 was incubated with the above agents or the vehicle alone for 30 s on ice. Fifteen milliliters of distilled water saturated with CO_2 by bubbling >1 h was added to the mixture, and the times until the pH of the mixture decreased from 8.6 to 6.3 were measured under the saturated condition. CA activity was expressed as $(T0 - T)/T0$ ($T0$ = time without CA II, T = time with CA II), the effect of each agent was expressed as the percentage of CA activity over that of the vehicle alone (control), and the ED_{50} values were determined by linear regression.

Assay for osteoclast differentiation in the mouse co-culture system

To isolate osteoblasts, calvariae dissected from 1- to 4-day-old mice were washed in PBS and digested with 1 ml of trypsin/EDTA (Life Technologies) containing 10 mg collagenase (Sigma type 7) for 10 minutes × 5 times, and cells from fractions 3–5 were pooled. Cells were plated in 6-multiwell dishes at a density of 5000 cells/cm^2 and grown to confluence in α-MEM containing 10% FBS. Osteoblasts (3×10^6 cells/well) prepared as described above and bone marrow cells (1×10^6 cells/well) from tibias of 8-week-old mice were co-cultured in 24-multiwell dishes containing α-MEM/10% FBS with or without FGF-2 (1 nM), Gas6 (1 nM), and soluble RANKL (30 ng/ml), and/or celecoxib, rofecoxib, JTE-522, acetazolamide, and SC-560 (all 1 μM) for 6 days with a medium change at 3 days. After 6 days of culture, cells were fixed with 3.7% (vol/vol) formaldehyde in PBS and ethanol-acetone (50:50, vol:vol) and stained at pH 5.0 in the presence of L(+)-tartaric acid using naphthol AS-MX phosphate in *N,N*-dimethyl formamide as the substrate. TRACP$^+$ multinucleated cells containing more than three nuclei were counted as osteoclasts.

Assay for mature osteoclast activity from M-BMMϕ culture

The activity of mature osteoclasts was measured using the M-BMMϕ culture above. After culture of bone marrow cells for 3 days, adherent M-BMMϕs were isolated and cultured as described above. Just before the fusion of cells, adherent cells were stripped by trypsin/EDTA, and further cultured on a dentine slice placed in each well of 96-well dishes containing α-MEM/10% FBS with or without FGF-2 (10 pM), Gas6 (1 nM), and soluble RANKL (30 ng/ml), and/or the agents above (all 1 μM). After 48 h of culture, cells were removed with 1N NH_4OH solution, and the dentine surface was stained with 0.5% toluidine blue. Total area was estimated under a light microscope with a micrometer to assess osteoclastic bone resorption using an image analyzer (System Supply Co., Nagano, Japan). At the same time, cells on a dentine slice in the independent culture were fixed and stained with TRACP as described above, and TRACP$^+$ multinucleated cells containing more than three nuclei were counted as mature osteoclasts.

To determine survival, osteoclasts generated as described above were cultured on a plastic dish for an additional 48 h. At 3, 6, 12, 24, and 48 h, the number of TRACP$^+$ and trypan blue–negative osteoclasts were counted.

Induction of AIA and drug administration in rats

AIA was induced in 6-week-old rats with subcutaneous injection of Freund's complete adjuvant containing 2% (wt/vol) *Mycobacterium butyricum* into the left hind-paw (day 0). From days 15 to 24, the indicated dosages (0.3–10 mg/kg/day) of celecoxib, rofecoxib, JTE-522, and acetazolamide suspended in 0.5% methylcellulose and 0.025% Tween-20 solution or the vehicle alone were administered orally twice a day (at 9:00 a.m. and 5:00 p.m.) at a volume of 5 ml/kg body weight.

Measurement of hind-paw swelling

The right hind-paw volume was measured with an instrument for plethysmography (MK-310; Muromachi Kikai Co., Tokyo, Japan) by vertically immersing the paw to the level of the proximal end of the lateral malleolus in a water-filled tub on day 25. The effect of each agent was expressed as the percent inhibition: the volume difference between normal and the drug-treated AIA divided by that between normal and the vehicle-treated AIA, and the dose of 50% inhibition determined by linear regression was expressed as the ED_{50} for each drug. After the measurement, the animals were killed, and the right hindlimbs were excised for the following radiological and histological examinations. The evaluations were performed by the same observer without knowledge of treatment.

Measurement of BMD

BMD (mg/cm^2) of the excised right hind-paws was measured by DXA using a bone mineral analyzer (QDR-2000; Hologic, Bedford, MA, USA). On the monitoring image of hindlimbs by lateral projection, each paw image was divided into five parts, and data from the first and second parts from the posterior heel side were represented as data for paw BMD. The effect of each agent was expressed as the percent inhibition: the BMD difference between normal and the drug-treated AIA divided by that between normal and the vehicle-treated AIA, and the dose of 50% inhibition determined by linear regression was expressed as the ED_{50} for each agent.

Measurement of serum concentration of type I collagen C-telopeptide

Immediately after the rats were killed, ~5 ml of blood was collected from the femoral vein. The blood was allowed to clot at room temperature for ~30 minutes after collection. The serum was separated by centrifugation at 1500*g* for 15

minutes at 4°C and stored at −80°C. Type 1 collagen C-telopeptide (CTx) concentration in the serum was measured using Rat Laps ELISA (Osteometer Bio Tech A/S, Herlev, Denmark), according to the manufacturer's instruction. Briefly, 20 μl of each sample was mixed with 100 μl of primary antibody in a preincubated ELISA plate and incubated overnight at 4°C. After 100 μl of peroxidase-conjugated goat anti-rabbit IgG antibody was added into each well, the mixture was incubated with 100 μl of the substrate solution. To stop the color reaction, 100 μl of stopping solution was added to each well, and the absorbance was measured at 450 nm with the reference at 650 nm. The effect of each agent was expressed as the percent inhibition: the difference between normal and the drug-treated AIA divided by that between normal and the vehicle-treated AIA, and the dose of 50% inhibition determined by linear regression was expressed as the ED_{50} for each agent.

Radiological scoring

Radiographs of the right hindlimbs were taken using a soft X-ray apparatus (CMB-2; Softex Co., Kanagawa, Japan). A 0–5 subjective grading system (0 = normal, 5 = the most severe) was used to evaluate bone destruction and periostitis, respectively, in the hind-paw, and the sum of the scores for the parameters was expressed as the radiological score (maximum 10). Radiographs of the adjuvant noninjected hindlimb were taken with a Softex-CMB X-ray unit (Softex Co.). The severity of bone damage was assessed blindly from the radiographs by grading the bone destruction and periostitis.

Histological scoring

After radiography, specimens were placed in 3.7% formaldehyde for 24 h and decalcified in 10% EDTA for 14 days. They were dehydrated with an increasing concentration of ethanol, embedded in paraffin, longitudinally sectioned into 4-μm-thick sections, and stained with H&E. A 0–5 subjective grading system (0 = normal, 5 = the most severe) was used to evaluate the overall change including synovial thickening (pannus formation) and joint destruction in the talo-tibial joint (maximum 5).

Statistical analysis

Statistical analysis was performed using Student's *t*-test or ANOVA. $p < 0.05$ was considered significant. Values are expressed as the mean ± SE.

RESULTS

Expressions of COX-2 and CA II during osteoclast differentiation

To investigate the expressions of COX-2 and CA II during osteoclast differentiation, these mRNA levels were examined in osteoclast precursor M-BMMϕs cultured in the presence of soluble RANKL and M-CSF without support of osteoblasts/stromal cells (Fig. 1). Because we extracted mRNA from cultured M-BMMϕs every day, various differentiation stages of osteoclastic cells were assumed to be included. COX-2 expression was not detected in any differentiation stage of osteoclasts as we previously reported in other osteoclastic cell lines,[10,11] indicating that COX-2 in osteoblasts/stromal cells, but not in cells of osteoclastic lineage, plays an important role in osteoclastic bone resorption. In the meantime, the CA II expression was detected at 4 days and increased at 5 days of culture, in accordance with the appearance of $TRACP^+$ multinucleated osteoclasts. This confirms that CA II is expressed predominantly in mature osteoclasts, but not in the precursors.

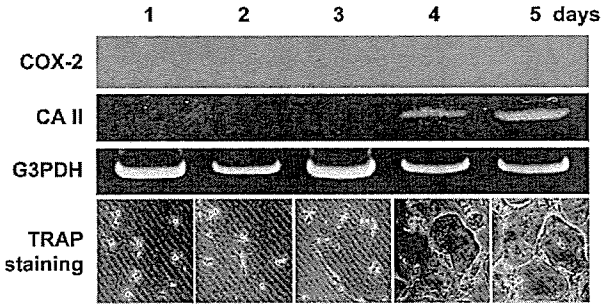

FIG. 1. Expressions of COX-2 and CA II during osteoclast differentiation. For osteoclast precursor cells, we used M-BMMϕs that were isolated from mouse bone marrow cells cultured in the presence of M-CSF. M-BMMϕs were further cultured with soluble RANKL and M-CSF for 1–5 days, and RNA extraction or TRACP staining was performed. The mRNA levels of COX-2 and CA II were determined by RT-PCR with that of G3PDH as a loading control. The PCR products for COX-2, CA II, and G3PDH were 939, 411, and 984 bp, respectively. $TRACP^+$ multinucleated osteoclasts stained in red were visible after 4 days of culture with the expression of CA II.

Inhibition of CA II activity by COX-2 selective agents

To study the inhibition of CA II activity by COX-2 selective agents and acetazolamide, a CA II inhibitor as a positive control, these drugs were incubated with CA II in the CO_2-saturated water (Fig. 2). The pH measurement revealed that the sulfonamide-type COX-2 inhibitors celecoxib and JTE-522 as well as acetazolamide exhibited inhibitory potency against CA II, whereas the methylsulfone-type rofecoxib did not, as previously reported.[24] The ED_{50} values of celecoxib, JTE-522, and acetazolamide were 97.7, 3.2, and 6.6 nM, respectively.

Effects of COX-2, COX-1, and CA II inhibitors on the differentiation of osteoclasts

We initially examined the actions of FGF-2, Gas6, and soluble RANKL on $TRACP^+$ multinucleated cell formation in the co-culture of mouse osteoblasts and bone marrow cells. As we reported previously, FGF-2 and soluble RANKL, but not Gas6, exhibited the stimulation of osteoclast formation[10,11,17] (Fig. 3A). When COX-2 inhibitors celecoxib, rofecoxib, and JTE-522, a CA II inhibitor acetazolamide, and a COX-1 selective inhibitor SC-560 were added to the co-cultures, only the COX-2 inhibitors with or without the CA II inhibitory potency clearly inhibited the FGF-2 action on osteoclast formation. Neither acetazol-

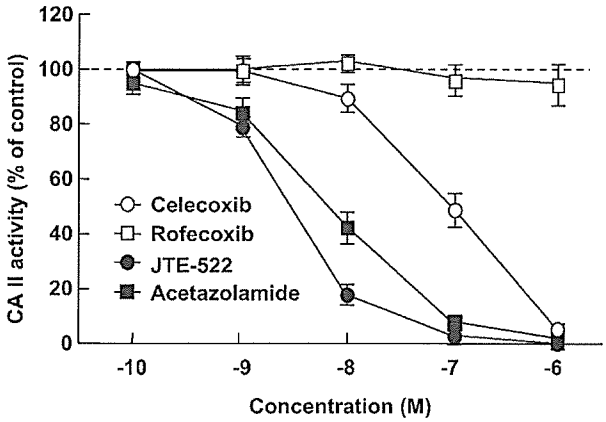

FIG. 2. Inhibition of CA II activity The inhibition of CA II activity by COX-2 selective agents celecoxib, rofecoxib, JTE-522, and a potent CA II inhibitor acetazolamide were determined by pH measurement in the mixture of each agent and CA II in the CO_2 saturated water. Data are expressed as means (symbols) ± SE (error bars) of the percentage of that of the vehicle alone (control) for three assays per group.

amide nor SC-560 altered the osteoclast formation. This indicates that COX-2, but not CA II or COX-1, is involved in the osteoclast differentiation of by FGF-2. In the meantime, none of the inhibitors reduced the soluble RANKL-stimulated osteoclast differentiation, confirming that RANKL lies downstream of COX-2 in the bone stimulatory signalings as previously reported.[6,10,11]

Effects of COX-2, COX-1, and CA II inhibitors on the activity of mature osteoclasts

To evaluate the effects of the inhibitors on the activity of mature osteoclasts, the pit area on a dentine slice resorbed by osteoclasts formed in the M-BMMϕ culture without osteoblasts/stromal cells was measured. We first confirmed our previous findings that FGF-2, Gas6, and soluble RANKL stimulated the resorbed pit area.[10,16,17] Among the inhibitors, celecoxib, JTE-522, and acetazolamide, which have the potency to inhibit CA II, abrogated the stimulations by the cytokines, whereas neither rofecoxib nor SC-560 without the CA II inhibitory potency altered them (Fig. 3B, top). These regulations by the cytokines and the CA II inhibitors were not caused by the change of the number of osteoclasts but by the regulation of each osteoclast activity, because none of the agents affected the number of $TRACP^+$ multinucleated osteoclasts on a dentine slice (Fig. 3B, middle). In fact, the effects of the agents on the pit area per osteoclast (resorbed pit area/osteoclast number on a dentine slice) showed a similar pattern to those on the resorbed pit area (Fig. 3B, bottom), indicating that CA II, but not COX-2 or COX-1, is involved in the activity of mature osteoclasts.

The lines of the in vitro results revealed the distinct effects of COX-2 inhibitors and CA II inhibitors on the differentiation of osteoclasts and the activity of mature osteoclasts, respectively.

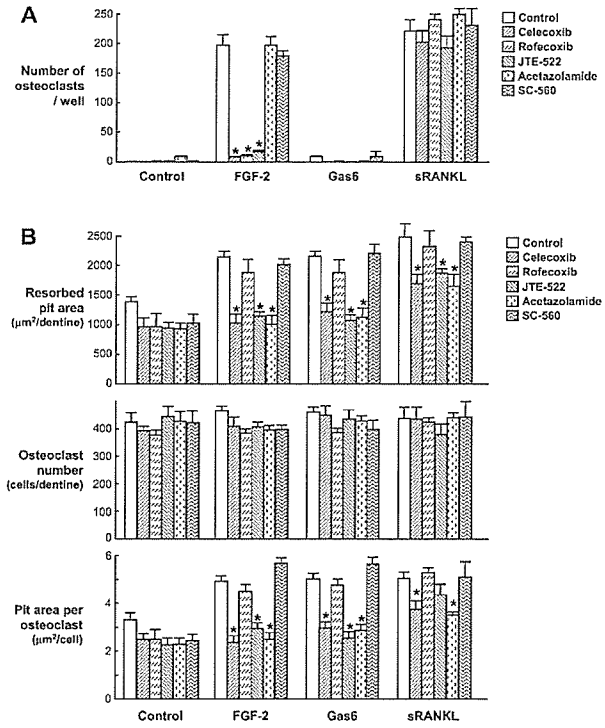

FIG. 3. Effects of COX-2, COX-1, and CA II inhibitors on (A) the differentiation and (B) activity of osteoclasts. (A) Osteoblasts from neonatal mouse calvariae and bone marrow cells from 8-week-old mice were co-cultured with or without FGF-2 (1 nM), Gas6 (1 nM), and soluble RANKL (30 ng/ml), and/or celecoxib, rofecoxib, JTE-522, acetazolamide, and SC-560 (all 1 μM) for 6 days. $TRACP^+$ multinucleated cells containing more than three nuclei were counted as osteoclasts. (B) Activity of mature osteoclasts was determined by the pit area on a dentine slice resorbed by osteoclasts generated in the M-BMMϕ culture without osteoblasts/stromal cells. The isolated osteoclasts were further cultured on a dentine slice with or without FGF-2 (1 nM), Gas6 (1 nM), and soluble RANKL (30 ng/ml), and/or the agents above (all 1 μM) for 48 h. The resorbed pit area was measured by toluidine blue staining on the dentine slice (top). At the same time, cells on a dentine slice in independent cultures were stained with TRACP, and the number of $TRACP^+$ multinucleated osteoclasts was counted (middle). As the bone resorptive activity of an individual osteoclast, the pit area per osteoclast (resorbed pit area/osteoclast number on a dentine slice) was also calculated (bottom). Data are expressed as means (bars) ± SE (error bars) for eight cultures per group. $^*p < 0.01$, significant inhibition by the agents.

Effects of COX-2 and CA II inhibitors on AIA bone destruction in vivo

Based on the in vitro results above, we examined the suppression of arthritic bone destruction by celecoxib, rofecoxib, JTE-522, and acetazolamide in AIA rats. Inflammation by AIA determined by the hind-paw swelling was dose-dependently inhibited by the COX-2 selective agents whether with or without the CA II inhibitory action (Fig. 4A). The ED_{50} values of celecoxib, rofecoxib, and JTE-522 were 0.26, 0.72, and 0.81 mg/kg/day, respectively. Bone destruction by AIA determined by the BMD loss of the hind-paw was also dose-dependently inhibited by the COX-2 selective agents with and without the CA II inhibitory ac-

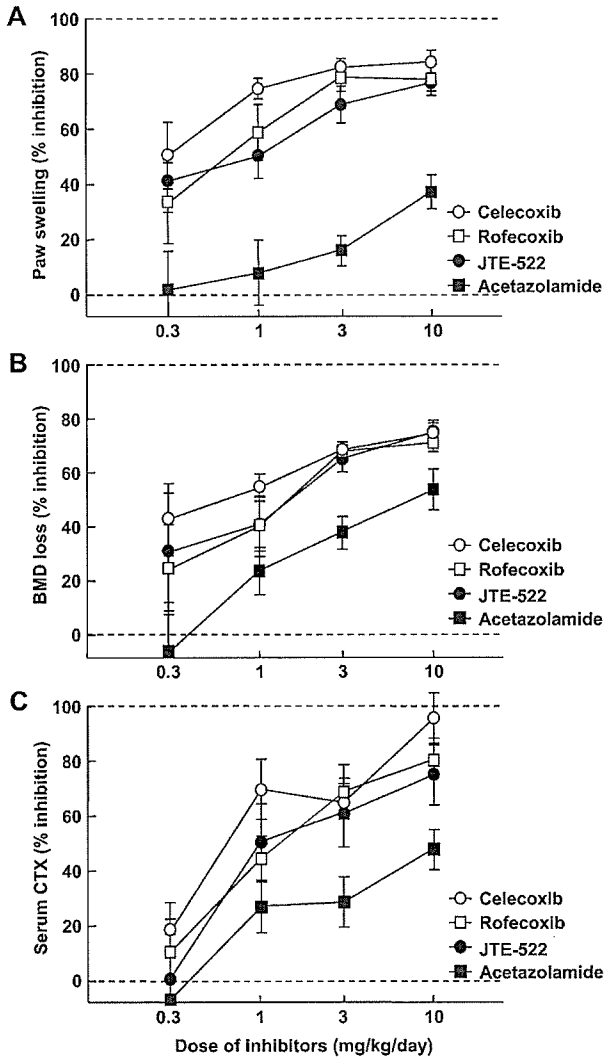

FIG. 4. Inhibitory effects of COX-2 and CA II–selective agents on (A) paw swelling, (B) BMD loss, and (C) a bone resorption marker CTx in AIA rats. AIA was induced in 6-week-old rats with subcutaneous injection of Freund's complete adjuvant containing *Mycobacterium butyricum* into the left hind-paw (day 0), and the indicated dosages (0.3–10 mg/kg/day) of celecoxib, rofecoxib, JTE-522, and acetazolamide were orally administered from day 15 to day 24. The right hind-paw volume was measured by a plethysmometer before killing the animals, and the serum CTx level by ELISA immediately after death on day 25. BMD of the excised right hind-paws was measured by DXA. Effects of the drugs on the parameters were expressed as the percent inhibition: the difference between normal and the drug-treated AIA divided by that between normal and the vehicle-treated AIA. Data are expressed as means (symbols) ± SE (error bars) for eight animals per group.

tion, and the ED_{50} values of celecoxib, rofecoxib, and JTE-522 were 0.69, 1.40, and 1.50 mg/kg/day, respectively (Fig. 4B). Similar results were obtained when BMC was used as a parameter for bone destruction (data not shown). In addition, serum level of CTx, a specific bone resorption marker, was also decreased by the COX-2 inhibitors: ED_{50} values of the above agents were 0.62, 1.14, and 0.86 mg/kg/day, respectively (Fig. 4C). Acetazolamide caused moderate inhibitions of paw swelling, BMD loss, and CTx level, although all were weaker than those of the COX-2 selective agents.

Figure 5A shows representative radiographs of hindlimbs and scorings of bone destruction and periostitis of normal and AIA rats with and without application of the COX-2 selective agents and acetazolamide. Bone destruction around the ankle joint and periostitis in the tibia and talus were markedly induced by AIA induction and were significantly reduced by all COX-2 selective agents with or without CA II inhibitory potency. Figure 5B shows the representative histological features of the talo-tibial joints and scorings of synovial thickening and joint destruction of normal and AIA rats with and without application of the agents above. Substantial trabecular bone loss in the tibia and talus, synovial thickening with cell proliferation, and decrease of the joint space were distinguished in the AIA vehicle-treated rats compared with normal rats. Here again, all COX-2 inhibitors significantly suppressed these disorders, and the effects were comparable between those with and without CA II inhibitory potency. Although acetazolamide tended to decrease both radiological and histological scores, the effects were weaker than those of COX-2 selective agents and were not significant as compared with that of the vehicle alone.

DISCUSSION

Based on a recent finding that COX-2 selective agents containing a sulfonamide moiety show an unexpected inhibition of CA II,[24] this study initially examined the CA II inhibitory potency of representative COX-2 selective agents and confirmed that the sulfonamide-type agents celecoxib and JTE-522 exhibited CA II inhibition, whereas the methylsulfone-type rofecoxib did not. In vitro assays for the differentiation of osteoclasts and the activity of mature osteoclasts clearly revealed that COX-2 selective agents with CA II inhibitory potency suppressed both differentiation and activity of osteoclasts, whereas those without potency reduced only osteoclast differentiation. Although this implies a superiority of COX-2 selective agents with CA II inhibitory potency over those without it as bone-sparing drugs, the present in vivo studies on AIA rats showed that all COX-2 selective agents similarly suppressed arthritic bone destruction with or without CA II inhibitory potency. Although inhibition of CA II alone by acetazolamide caused a moderate suppression of bone destruction, the effect was weaker than that by COX-2 inhibition. The lines of these results indicate the importance of suppression of osteoclast differentiation by COX-2 inhibition rather than suppression of mature osteoclast activity by CA II inhibition, at least for the treatment of AIA bone destruction.

The predominance of osteoclast differentiation over osteoclast activation in the mechanism of arthritic bone destruction is in accordance with accumulated evidence showing the pivotal role in RA bone destruction of bone resorptive cytokines TNF-α, IL-1, and IL-6, which stimulate osteoclast differentiation through induction of RANKL with little effect on mature osteoclast activity.[29] Hence,